Medizinische Fakultät

Der

Universität Duisburg-Essen

Aus der Klinik für Neurochirurgie

Knockdown von PDCD10 führt in Glioblastom- und Endothelzellen zu Tumorwachstum über die Aktivierung der EphB4-Kinase *in vitro* und *in vivo*

Inaugural-Dissertation

Zur

Erlangung des Doktorgrades der Medizin

durch die Medizinische Fakultät

der Universität Duisburg-Essen

Vorgelegt von

Xueyan Wan

aus Wuhan, V. R. China

2020

DOI: 10.17185/duepublico/74232
URN: urn:nbn:de:hbz:464-20210526-104433-4

Dekan: Herr Univ.-Prof. Dr. med. J. Buer

1. Gutachter: Frau Prof. Dr. rer. nat. Y. Zhu

2. Gutachter: Herr Prof. Dr. rer. nat. A. Schramm

Tag der mündlichen Prüfung: 18. März 2021

Publication

1. Nickel AC, **Wan XY**, Saban DV, et al. Loss of programmed cell death 10 activates tumor cells and leads to temozolomide-resistance in glioblastoma. *J Neurooncol.* 2019, 141: 31-41 (Equal contribution as first author).
2. **Wan XY,** Saban DV, Kim SN, et al. PDCD10-deficiency promotes malignant behaviors and tumor growth via triggering EphB4 kinase activity in glioblastoma. Front Oncol. 2020, doi: 10.3389/fonc.2020.01377. eCollection 2020.

Poster

Loss of PDCD10 stimulates glioblastoma cells in vitro and promotes tumor growth in vivo. Forschungstag 2017, Essen, 17.11.2017

Meeting

Lecture in 69th Annual meeting of German Neurosurgery (DGNC) 3–6 June 2018, Münster

To

my family

Contents

1. Introduction 7

1.1 Glioblastoma (GBM) 7

1.2 Programmed cell death 10 (PDCD10) 8

1.2.1 The role of PDCD10 in endothelial cells 8

1.2.2 The function of PDCD10 in tumor 9

1.3 The function of EphB4 in tumor 11

2. Materials and Methods 12

2.1 Materials 12

2.1.1 Materials for the culture of PDCD10-knockdown (shPDCD10) GBM cells 12

2.1.2 Materials for human GBM xenograft model 12

2.1.3 Materials for phenotype studies of GBM cells and HUVECs 13

2.1.4 Materials for RNA extraction, cDNA synthesis and real time-PCR . 13

2.1.5 Materials for Western blotting 14

2.1.6 Materials for Enzyme-linked immunosorbent assay (ELISA) 14

2.1.7 Materials for immunochemistry staining 14

2.1.8 Materials for protein array 14

2.2 Methods 14

2.2.1 The culture of shPDCD10 cells and the treatment 14

2.2.2 Phenotype studies of T98g cells after knockdown of PDCD10 15

2.2.3 Phenotype studies of HUVECs after treatment of conditioned medium from shPDCD10 GBM cells 17

2.2.4 RNA extraction, cDNA synthesis and real-time PCR (RT^2-PCR) 19

2.2.5 Western blotting 19

2.2.6 Enzyme-linked immunosorbent assay (ELISA) 22

2.2.7 Protein array 22

2.2.8 Human GBM xenograft model 23

2.2.9 Statistical analysis 24

3. Results 25

3.1 Confirmation of PDCD10 knockdown and activation of EphB4 in PDCD10 knockdown GBM cells 25

3.2 Knockdown of PDCD10 activated GBM cells, which was rescued by the specific kinase inhibitor of EphB4 (NVP-BHG712) 27

3.2.1 Knockdown of PDCD10 promoted proliferation of T98g cells, which

was reversed by NVP-BHG712 treatment 27
3.2.2 Knockdown of PDCD10 enhanced adhesion of T98g cells, which was suppressed by the treatment of NVP-BHG712 28
3.2.3 Knockdown of PDCD10 activated migration of T98g cells, which was inhibited by the treatment of NVP-BHG712 29
3.2.4 Knockdown of PDCD10 stimulated T98g cell invasion, which was hindered by the treatment of NVP-BHG712 31
3.3 Conditioned medium from shPDCD10 GBM cells triggered endothelial cells (ECs) 32
3.3.1 Conditioned medium from shPDCD10 T98g cells stimulated HUVECs growth 32
3.3.2 Conditioned medium from shPDCD10 GBM cells promoted HUVECs adhesion 33
3.3.3 Conditioned medium from shPDCD10 GBM cells enhanced HUVECs migration 33
3.4 Knockdown of PDCD10 promoted tumor progression *in vivo*, which was suppressed by the treatment of NVP-BHG712 35
3.4.1 Knockdown of PDCD10 promoted tumor progression *in vivo*, which was suppressed by the treatment of NVP-BHG712 35
3.4.2 Knockdown of PDCD10 activated the proliferation of shPDCD10 U87 cells *in vivo,* which was inhibited by the treatment of NVP-BHG712 38
3.4.3 Knockdown of PDCD10 promoted the neo-angiogenesis of shPDCD10 U87 cells *in vivo,* which was rescued by NVP-BHG712 39
3.5 Knockdown of PDCD10 in GBM cells stimulated the release of pro-angiogenic factors 40
4. Discussion 43
5. Summary 49
Zusammenfassung 50
6. Reference 51
7.1 Abbreviation 61
7.2 Figure titles 64
7.3 Table titles 65
8. Acknowledgements 66
9. List of publication 67
10. Curriculum Vitae 68

1. Introduction

1.1 Glioblastoma (GBM)

Glioma, an annual incidence of 5–7 cases out of 100,000 people, is the most common group of primary brain tumors in adult (Alexander et al, 2017; Alifieris et al, 2015; Cloughesy et al, 2014; Vollmann-Zwerenz et al, 2020). Based on certain pathological features, such as nuclear atypia, mitotic activity, endothelial proliferation, necrosis and proliferative index, the gliomas are assigned a grade from I to IV according to World Health Organization (WHO) grading system and grade IV astrocytoma is regarded as glioblastoma (GBM) (Alifieris et al, 2015; Marquet et al, 2007). Traditionally, GBM is usually classified into 2 major classes as primary and secondary GBM. Most of the cases belong to the first group, without a history of low-grade glioma and it develops from normal glial cells by multistep tumorigenesis. The secondary GBM, accounting for about 10%, is developing by progression from low-grade tumors, which takes about 4–5 years. Even though the clinical course and the potential pathways underlying development are different, both are characterized by high vascularization and numerous necrotic cores surrounding with 'pseudopalisades' and do not show morphological differences (Alifieris et al, 2015).

The most common symptoms of GBM include headaches, numbness, vision disturbances, alteration of language, mood disorders, and mild memory disorders depending on the localization and size of the tumor as well as the intracranial pressure (Urbanska et al, 2014). Because of these unspecific signs, glioma sometimes is misdiagnosed as other diseases at initial stage, such as inflammation, infection and so on. Fortunately, in clinical settings, magnetic resonance imaging (MRI) is usually used to differentiate these diagnoses and provide detailed information of the patient's brain and is considered as a helpful tool to diagnose GBM. However, definitive diagnosis is based on histopathological examination from resected or biopsied tumors, using traditional histological, cytological, and histochemical methods. In some cases, molecular analysis could help clarify the diagnosis.

Currently, the etiology and pathogenesis of GBM are not fully elucidated (Thomas et al, 2014). In an attempt to better understand the tumorigenesis of this disease, primary glioblastoma has been undergoing comprehensive analysis by the Cancer Genome Atlas (TCGA) and the results reveal a lot of genetic abnormalities in GBM, including loss of CDKN2A, RB1, and TP53 tumor suppressor genes, mutations in the IDH1, ATRX, and p53 genes, as well as activation of oncogenic pathways such as receptor tyrosine kinases (RTKs), PI3K–AKT–mTOR as well as RAS–MAPK signaling pathways (Alifieris et al, 2015; Cloughesy et al, 2014). According to the findings of TCGA, 4 transcriptional subtypes of this disease are classified, namely classical, proneural, mesenchymal, and neural (Verhaak et al, 2010). Further studies show that patients with mutations in isocitrate dehydrogenase (IDH) (Turkalp et al, 2014) and O^6-methylguanine-methyltransferase (MGMT) promoter methylation (Hegi et al, 2005) have a better prognosis. Meanwhile, some new therapies are also emerging, such as targeting pathways of tumorigenesis, anti-angiogenic therapy, immunotherapy, and so on (Thomas et al, 2014). Unfortunately, little achievement has been made toward improving the prognosis of the patients no matter what the tumor's molecular characteristics is or which treatment is applied. Based on recent reviews regarding the GBM, the median patient survival is still less than 15 months with a 5-year survival rate less than 5% even though administrated maximal-safe surgical resection, followed by radiotherapy with concomitant temozolomide (TMZ) and then adjuvant TMZ (Alexander et al, 2017; Alifieris et al, 2015; Cloughesy et al, 2014). Given the poor survival with currently standard treatments, new therapeutic options for glioblastoma are urgently needed. Thus, increasing attention still has been focused on exploring new therapeutic methods that specifically target the regulatory genes in glioblastoma to get better survival of the patients.

1.2 Programmed cell death 10 (PDCD10)

1.2.1 The role of PDCD10 in endothelial cells

Programmed cell death 10 (PDCD10) was initially named as TFAR15 (TF-1 cell apoptosis-related gene 15) in 1999 through a screening for gene expression after induction

of apoptosis in TF-1 premyeloid cell line (Wang et al, 1999). PDCD10 encodes an evolutionarily conserved protein, which is ubiquitously expressed in nearly all human tissues and various types of cells including neuronal, glial, and endothelial cells (ECs) (Petit et al, 2006). PDCD10 is essential for vascular development and post-natal vessel maturation. Loss-of-function mutations in PDCD10 is usually detected in the familial form of cerebral cavernous malformation (CCM), one of the most common vascular lesions in the central nervous system involving aberrant angiogenesis (Bergametti et al, 2005; Jenny Zhou et al, 2016). Further studies demonstrate that mutation of PDCD10/CCM3 leads to the earlier onset of CCM and the most aggressive haemorrhage in CCM (Shenkar et al, 2015). Thus, the vascular function of PDCD10 has attracted a lot of attention and has been intensively investigated in the past decade. It is demonstrated that silencing PDCD10 promotes endothelial proliferation, migration and tube sprouting (You et al, 2017) and overexpression of PDCD10 has the opposite effect (Schleider et al, 2011) in ECs. Nowadays, the underlying molecular mechanism of CCM caused by mutant PDCD10 is gradually addressed, including impairing DLL4-Notch signaling (You et al, 2013), exocytosis of angiopoietin-2 (Jenny Zhou et al, 2016), activation of RhoA, and increased vessel permeability (Borikova et al, 2010), and increased activity of MEKK3 (Zhou et al, 2016). Moreover, as a pleiotropic protein, PDCD10 can also interact with a variety of signaling proteins, such as p-Akt, p38, p-Erk, VEGFR2, STK24/25, MST4, RhoA, Dll4-Notch, and SMAD, thereby regulating multiple functions, including migration, angiogenesis, vascular permeability, apoptosis and senescence, oxidative metabolism and Golgi complex polarization (Draheim et al, 2014; Fidalgo et al, 2010; Madsen et al, 2015; Schleider et al, 2011; Zheng et al, 2010; Zhu et al, 2010). More recently, loss of endothelial PDCD10 has been shown to activate MEKK3-KLF2/4 and mTOR signalling pathways resulting in defects of the vascular development (Zhou et al, 2016) and defective autophagy (Marchi et al, 2015), respectively.

1.2.2 The function of PDCD10 in tumor

Many researchers focus on the vascular function of PDCD10 and the potential mechanism

of PDCD10 mutation in CCM since the mutation of PDCD10 is one cause of familial CCM (Bergametti et al, 2005; Shenkar et al, 2015). Some groups begin to investigate the function of tumor-originated PDCD10 because increasing data suggest that PDCD10 might be involved in tumorigenesis. The following studies indicate that the expression of PDCD10 is altered in a variety of malignant tumors. For example, PDCD10 is upregulated in prostate cancer, colorectal cancer and non-small cell lung cancer (NSCLC) tissues (Barrier et al, 2005; Fu et al, 2016; Yang et al, 2017). Other tumor types, like glioblastoma, show a down-regulation of PDCD10 (Lambertz et al, 2015). Although mounting evidence uncover the function of PDCD10 in the tumor, it still remains controversial under intense study and it seems to be cell and content dependent as demonstrated by ample studies of PDCD10 overexpression (Barrier et al, 2005; Chen et al, 2009; Lin et al, 2010; Schleider et al, 2011; Yang et al, 2017) or PDCD10 knockdown (Fu et al, 2016; He et al, 2010; Louvi et al, 2011; Zhang et al, 2016; Zheng et al, 2010; Zhu et al, 2016) in which different cell types respond in opposite directions. For example, Barrier *et al* (Barrier et al, 2005) demonstrated that over-expression of PDCD10 was associated with poor prognosis of colorectal cancer patients. Fu et al (Fu et al, 2016) also showed that down-regulation of PDCD10, a direct target of miR-103, could suppress prostate cancer proliferation and migration. Ma *et al* (Ma et al, 2007) also pointed out that PDCD10 could promote prostate cancer cell proliferation and transformation by activating MST4 activity and may be involved in the Erk pathway. These data suggest that a potential tumor promotion function of PDCD10. Nevertheless, some other studies demonstrate a potential tumor suppressor-like function of PDCD10. A study indicated that the down-regulation of PDCD10 modulated by miRNA-425-5p was involved in chemo-resistance in colorectal cancer cells (Zhang et al, 2016). Furthermore, patients carrying heterozygous mutations of PDCD10 leading to truncated or non-functional PDCD10 protein were harboring an increased risk to develop meningioma (Fauth et al, 2015; Labauge et al, 2009; Riant et al, 2013). Recently, the downregulation of PDCD10 was demonstrated to be associated with chemo-resistance in colorectal cancer cells (Zhang et al, 2016). How these conflicting data can

be reconciled remains to be investigated.

1.3 The function of EphB4 in tumor

Ephrin type-B receptor 4 (EphB4), a member of the tyrosine kinase family, is preferentially expressed in venous endothelial cells (ECs). EphB4 binds specifically with its ligand ephrinB2 via direct cell-cell contact, resulting in EphB4-ephrinB2-complex dimerization and subsequent induction of bi-directional signaling. Upon engagement of EphB4 with ephrinB2, EphB4 becomes auto-phosphorylated on its kinase domain, thereby activating the kinase-dependent forward signaling; the reverse signaling is activated upon ephrinB2 tyrosine phosphorylation through recruitment of itself (Murai et al, 2003). This ligand-receptor interaction plays important roles in diverse cell biological processes, such as cell morphogenesis (Klein, 2004), cell adhesion/repulsion (Mellitzer et al, 1999), and angiogenesis (Cheng et al, 2002), and is also involved in tumor progression (Heroult et al, 2006). EphB4 is overexpressed in various types of solid tumors, such as colon cancer (Kumar et al, 2009), bladder cancer (Xia et al, 2006), breast cancer (Brantley-Sieders et al, 2011), esophageal cancer (Hasina et al, 2013), lung cancer (Ferguson et al, 2013) and mesothelioma (Liu et al, 2013). It is noteworthy that EphB4 expression increased in human gliomas in a grade-dependent manner and was also associated with the neo-vascularization and with tumor progression and poor prognosis in GBM patients (Chen et al, 2013; Tu et al, 2012). These data suggest EphB4 is a critical intermediator in GBM.

We have previously investigated the angiogenic and apoptotic functions of PDCD10 in vascular ECs and the underlying molecular mechanism (You et al, 2013; You et al, 2017; Zhu et al, 2010). By siRNA transfection- and lentiviral shRNA transduction mediated knockdown methods, we demonstrated that loss of endothelial PDCD10 stimulated endothelial proliferation, adhesion, migration, and tube formation *in vitro* and promoted neo-angiogenesis *in vivo* through the activation of EphB4-forward signaling (You et al, 2017). Further study of the interaction between ECs and GBM cells (TCs) indicated that PDCD10-ablation in ECs activated proliferation-, adhesion-, invasion- and

migration of TCs *in vitro* and promoted neo-angiogenesis and tumor growth in xenograft models (Zhu et al, 2016). Based on these findings together with the previous observation that PDCD10 was absent not only in the majority of ECs but also in TCs of the tumor tissue resected from GBM patients (Lambertz et al, 2015), we recently extended our research to study the role of TC-originated PDCD10 in GBM.

The aims of the present study include: 1. to investigate the role of PDCD10 in GBM cells and the interaction of GBM cells and endothelial cells; 2. to explore the potential mechanism of these effects. To this end, cell phenotype study of tumor cells and ECs is performed in PDCD10-knockdown (shPDCD10) GBM cells. Tumor growth is investigated in a human GBM xenograft mouse model. The underlying mechanism and the potential therapy are explored.

2. Materials and Methods

2.1 Materials

2.1.1 Materials for the culture of PDCD10-knockdown (shPDCD10) GBM cells

The PDCD10-knockdown GBM cells were previously established in our research laboratory. HUVEC was purchased from Cascade Biologics. The following materials were applied in cell culture.

Dulbecco's modified Eagle's medium	Thermo Scientific, Schwerte, Germany
Minimum Essential Medium Eagle	Sigma, Munich, Germany
Fetal bovine serum	Thermo Scientific, Schwerte, Germany
Glutamine	Sigma, Munich, Germany
non-essential amino acids	Sigma, Munich, Germany
sodium pyruvate	Thermo Scientific, Schwerte, Germany
ECGM+supplements	PromoCell, Heidelberg, Germany
Doxycyclin	Sigma, Munich, Germany
puromycin	Sigma, Munich, Germany

2.1.2 Materials for human GBM xenograft model

Female nude mice of 4-6 weeks old were obtained from Duisburg-Essen University

Medical College and fed in a specific pathogen-free animal environment. All animal experiments were carried out strictly according to the approved ethics contract with "Landesamt für Natur, Umwelt und Verbraucherschutz, the State of Nordrhein-Westfalen, Germany" (Nr.: 84-02.04. 2012.A348). Except for the animals, the following materials were applied in the experiments.

Matrigel	BD, Heidelberg, Germany
Fibrinogen	Sigma, Munich, Germany
Recombinant Human VEGF165	R&D, Wiesbaden, Germany
Recombinant Human FGF basic 146aa	R&D, Wiesbaden, Germany
Thrombin	Sigma, Munich, Germany
Doxycyclin	Sigma, Munich, Germany
NVP-BHG712	Sigma, Munich, Germany
1-methyl-2-pyrrolidone	Sigma, Munich, Germany
polyethylene glycol 300	Sigma, Munich, Germany

2.1.3 Materials for phenotype studies of GBM cells and HUVECs

WST-1	Roche, Mannheim, Germany
MTT	Life technology, Darmstadt, Germany
24-well transwell insert (8 μm)	Greiner Bio-One, Frickenhausen, Germany
Crystal Violet	Sigma, Munich, Germany
Sodium dodecyl sulfate (SDS)	Sigma, Munich, Germany
Matrigel	BD, Heidelberg, Germany
Methylcellulose	Sigma, Munich, Germany
NVP-BHG712	Sigma, Munich, Germany

2.1.4 Materials for RNA extraction, cDNA synthesis and real time-PCR

innu PREP RNA mini kit	Analyticjena, Berlin, Germany
iScript cDNA synthesis kit	Bio-Rad, Munich, Germany
SYBR green supermix	Bio-Rad, Munich. Germany

2.1.5 Materials for Western blotting

Protease inhibitor	Sigma, Munich, Germany
Phosphatase inhibitor	Sigma, Munich, Germany
Micro BCA™ Protein assay kit	Thermo Scientific, Schwerte, Germany
Albumin standard	Thermo Scientific, Schwerte, Germany
SDS	Sigma, Munich, Germany
Glycerol	Sigma, Munich, Germany
Ponceau S	Sigma, Munich, Germany
Tween 20	Sigma, Munich, Germany
Rabbit anti-PDCD10 (Cat# A57392)	Atlas Antibodies AB, Stockholm, Sweden
Rabbit anti-GAPDH (Cat# 2118S)	Cell signaling, Frankfurt am Main, Germany
Mouse anti-EphB4(Cat# sc-130081)	Santa Cruz, Heidelberg, Germany
SignalFire™ ECL reagent	Cell signaling, Frankfurt am Main, Germany

2.1.6 Materials for Enzyme-linked immunosorbent assay (ELISA)

EphB4 ELISA kit	R&D, Wiesbaden, Germany

2.1.7 Materials for immunochemistry staining

mouse anti-Ki67	Zytomed, Berlin, Germany
Mouse anti-CD31(Cat# M0823)	Dako, Hamburg, Germany
Retrieval solution	Dako, Hamburg, Germany

2.1.8 Materials for protein array

Human angiogenesis assay kit	R&D Systems, Wiesbaden, Germany

2.2 Methods

2.2.1 The culture of shPDCD10 cells and the treatment

The lentiviral shRNA vector for human PDCD10 (shPDCD10, catalog# TL302576) and the empty vector (EV, catalog# TR30021) from OriGene were used to achieve knockdown of *PDCD10* in T98g cells. The transfected T98g cells (EV and shPDCD10) were maintained in minimum essential medium Eagle (MEME) supplemented with 2 mM Glutamine, 1% non-essential amino acids, 1% sodium pyruvate, 10% FBS, and 1 µg/ml

puromycin. The knockdown of the *PDCD10* gene in U87 was achieved by the doxycycline inducible TRIPZ lentiviral shRNA vector for human PDCD10 (shPDCD10, Clone ID: V2THS_217165); and the empty vector (EV, catalog# RHS4750) was used as a control. The transfected U87 cells (EV and shPDCD10) were cultured in Dulbecco's modified Eagle's medium (DMEM) containing 10% fetal bovine serum (FBS), 1 µg/ml doxycycline (dox), and 1 µg/ml puromycin. HUVECs were maintained in Endothelial Cell Growth Medium (ECGM) with supplements. Cells were sub-cultured for experiments when they reached 70-80% of confluence and less than 8^{th} passage of HUVECs was applied in the following experiment. To inhibit EphB4 kinase activity, NVP-BHG712 (NVP), a specific EphB4 kinase inhibitor, was purchased from Sigma and dissolved in DMSO at 10 mM as a stock solution. Cells were treated with a solution containing 10 or 25 nM of NVP for different periods as indicated for each experiment.

2.2.2 Phenotype studies of T98g cells after knockdown of PDCD10

The phenotype studies of T98g cells were performed according to our recent publication (Nickel et al, 2019).

2.2.2.1 Proliferation assay

T98g cells (2.0×10^3/well) were seeded in a 96-well plate and incubated for 24 h, after that, the medium was refreshed with or without 25 nM NVP and the cells were continued to incubate for 24 h. WST-1 was used to detect the proliferation. The absorbance was detected at 450 nm by a plate reader.

2.2.2.2 Migration assay

Scratch assay and spheroid migration assay were performed to evaluate the cell motility of GBM cells after a stable knockdown of PDCD10.

For the scratch assay, 3×10^5 cells were plated into 35 mm PD. When the confluence of cells reached about 90 %, 2 or 3 scratch lines were made with a 100 µl tip across the marked lines, followed by washing twice by the medium and refreshing the medium with or without 10 nM of NVP. Six fields per dish (two dishes per group) were recorded immediately as 0 h and 24 h after scratching. The cell-free area was quantified by using "MRI_Wound_healing_Tool" in Image J software and the migrated area reflexes the

closed area when of the area at 0 h time point substrate the area measured at 24 h after scratching.

Spheroid migration assay was performed to mimic the multi-directional migration of cells. A total of 1.0 x 10^3 T98g transduced cells were suspended in a medium containing 20% methylcellulose and plated into U shape 96-well plates to generate the spheroids. After incubation overnight, the formation and quality of the spheroids were evaluated under 5 magnification. Nicely formed spheroids (round and regular) were carefully picked up and reseeded into a flat shape 96-well plate precoated with matrigel (0.5 mg/ml). 100 µl medium with or without 25 nM NVP was added into each well. The spheroids were then photographed by an inverse fluorescence microscopy after incubation for indicated time and the spheroid diameter was measured by Image J software.

2.2.2.3 Adhesion assay

For adhesion assay, 50 µl Matrigel solution (0.5 mg/ml) was used to pre-coat the 96-well plate and let it dry at 4 °C one day before the experiment. The pre-coated plate was hydrated with 100 µl of serum-free medium for at least 30 min at 37°C before use. After preparation of the plate, a total of 1 × 10^4 GBM cells in 100µl medium with or without 25 nM NVP were plated and incubated for 90 minutes. The non-adhesion cells were gently removed by washing with PBS. The adhesion cells were fixed and stained with 0.5% of crystal violet in methanol for 10 min at room temperature and destained with 200 µl of sodium dodecyl sulfate (SDS, 1%) for 10 min at room temperature. The absorbance of the migrated cells was detected at 550 nm by a plate reader.

2.2.2.4 Transwell invasion assay

The invasion assay was performed using a 24-well transwell plate. The insert of the transwell system (8µm-pore size) was precoated with 0.5 mg/ml matrigel in advance. Before the experiment, the pre-coated insert was hydrated with 200 µl of serum-free medium for 1 hour at 37°C in the incubator. T98g cells were starved overnight and the next day 1×10^5 cells were suspended in serum-free medium with or without 25 nM NVP and seeded into the 24-well transwell insert. Media containing 10% FBS was added into

the lower chamber. After incubation for 48 h, the uninvaded cells were gently removed by a cotton swab and the invaded cells were stained with 0.5% crystal violet and destained with 1% sodium dodecyl sulfate followed by measuring the absorbance at 550 nm with a plate reader.

2.2.3 Phenotype studies of HUVECs after treatment of conditioned medium from shPDCD10 GBM cells

2.2.3.1 Conditioned medium (CM)

A total of 3×10^6 EV- or shPDCD10-U87 or T98g cells were suspended in 10 ml DMEM or MEME medium without puromycin and plated onto the 100 mm PD, respectively. After culture for 3 days, the media was collected and centrifuged at 2000 g for 10 min followed by aliquoting and storing at -80°C for later use. The CM containing 50% of the collected medium and 50% of ECGM with supplements was applied for the following experiments. The EVCM was composed of the 50% collected media from EV-U87 or EV-T98g cells and 50% of ECGM with supplements, and the shCM was made up of 50% collected media from shPDCD10-U87 or shPDCD10-T98g cells and 50% of ECGM with supplements.

2.2.3.2 Viability assay in CM-treated HUVECs

A total of 4000 cells per well HUVECs were seeded in a 96-well plate and incubated overnight, followed by refreshing the CM and continued to culture the cells for 24 h. The viability of HUVECs was evaluated by MTT assay. MTT (3-(4,5-Dimethylthiazol-2-yl)-2,5-Diphenyltetrazolium Bromide) (5 mg/ml) (Life technology, Darmstadt, Germany) was added to the culture and incubated for 3 h. To dissolve the MTT formazan, 150 µl of MTT solvent (4 mM HCl, 0.1% NP40 in isopropanol) was added to each well and the plate was incubated on an orbital shaker for 15 min at room temperature. The absorbance was detected at 590 nm in a plate reader.

2.2.3.3 Migration assay in conditioned medium-treated HUVECs

Scratch assay and spheroid migration assay were performed to evaluate the cell motility of HUVECs after treated with CM.

Scratch assay

For the scratch assay, 3×10^5 cells were plated into 35 mm PD. When the confluence of cells reached about 90%, 2 scratch lines were made with a 100 µl tip across the marked lines, followed by washing twice with media and refreshing the CM. Four fields per dish (two dishes per group) were recorded immediately as 0 h and 12 h after scratching. The cell-free area was quantified by using "MRI_Wound_healing_Tool" in Image J software and the migrated area reflexes the closed area when of the area at 0 h time point substrate the area measured at 12 h after scratching.

Spheroid migration assay

Spheroid migration assay was performed to mimic the multi-directional migration of cells. A total of 500 HUVECs per well were suspended in medium containing 20% methylcellulose and plated into U shape 96-well plates to generate the spheroids. After incubation overnight, the formation and quality of the spheroids were evaluated under 5 magnification. The formed spheroids (round and regular) were carefully picked up and reseeded into a flat shape 96-well plate precoated with matrigel (0.5 mg/ml). The volume of 100 µl CM was added into each well. The spheroids were then photographed by an inverse fluorescence microscopy after incubation for indicated time points and the spheroid diameter (the shortest and longest dimeters were measured and the mean diameter was calculated) was measured by Image J software.

2.2.3.4 Adhesion assay in CM-treated HUVECs

For adhesion assay, 50 µl 0.2% gelatin solution was used to precoat the 96-well plate and let it dry at 4 °C one day before the experiment. The pre-coated plate was hydrated with 100 µl of serum-free medium for at least 30 min at 37°C before use. After preparation of the plate, 1×10^4 HUVECs in CM were plated and incubated for 90 minutes followed by once wash with warm PBS. The adhesion cells were fixed and stained with 0.5% of crystal violet in methanol for 10 min at room temperature and destained with 200 µl of 1% SDS for 10 min at room temperature. The absorbance of the migrated cells was detected at 550 nm by a plate reader.

2.2.4 RNA extraction, cDNA synthesis and real-time PCR (RT^2-PCR)

Total RNA was extracted using the innuPREP RNA mini kit and the cDNA was synthesized using the iscript cDNA kit according to the manufacturer's instructions. The PCR reaction mixture was prepared to a final volume of 15 µl comprising of 6 µl of cDNA template (4 ng/µl), 7.5 µl of SYBR green supermix (Bio-Rad, Munich, Germany), 0.3 µl of forward and reverse specific primers (10 µM) and RNAse-free H_2O. RT^2-PCR was performed on iQ5 PCR instrument (Bio-Rad, Munich, Germany) by using 3 step program parameters as follows: 15 min at 95°C for denaturation, and then 40 cycles of amplification at 95°C for 30 sec, annealing at 60°C for 30 sec and 72°C for 50 sec, 95°C for 1 min, and 55-95°C with a heating rate of 0.5°C every 10 sec. Glyceraldehyde-3-phosphate dehydrogenase (GAPDH) was stably detected and was used as the reference gene. The mRNA expression level of the gene of interest was normalized against GAPDH. The relative expression of the target gene was calculated by $2^{-\Delta\Delta Ct}$ method as described previously. Primer sequences and annealing temperature for individual genes are listed in Table 1.

Table 1 Primer sequences for real-time RT-PCR

Primer	Sequence	Ta (°C)
PDCD10		**60**
for.	TGG CAG CTG ATG ATG TAG	
rev.	TCG TGC CTT TTC GTT TAG	
EphB4		**58**
for.	TGT GTT GGA GGG AAC CTG	
rev.	GGG CCC CTG TTT CAA CTT G	
GAPDH		**60**
for.	AGC CAC ATC GCT CAG ACA	
rev.	GCC CAA TAC GAC CAA ATC C	

for. forward; rev. reverse. Ta. Annealing temperature

2.2.5 Western blotting

Buffers and gels preparation

Loading buffer (5×) preparation

Content	Volume (mL)
Glycerol	1
10% SDS	3.0
2-Mercaptoethanol	2.5
0.05% Bromphenol blue	2.5
Tris (0.5 M, pH = 6.8)	2.5

Separation Gel preparation (12%)

Content	1 gel (µl)
Separating buffer*	2625
30% acrylamide/0.8% bisacrylamid	3000
10% APS	25
TEMED	7.5
Distilled water	2625

*Separating buffer: 1.5 M of Tris, pH = 8.8, 0.4% of SDS.

Collecting gel preparation

Content	1 gel (µl)
Collecting buffer*	625
30% acrylamide/0.8% bisacrylamid	375
10% APS	25
TEMED	2.5
Distilled water	1500

*Collecting buffer: 0.5 M of Tris, pH = 6.8, 0.4% of SDS.

Electrophoresis buffer

Content	Volume /weight
Tris	3.0 g
Glycine	14.4 g
SDS	1.0 g
Distilled water	Add to 1L

Blotting buffer

Content	Volume /weight
Tris	1.82 g
Methanol	100 mL
SDS	1.0 g
Distilled water	Add to 0.5 L

Protein extraction

For total protein extraction, cells were lysed in a lysis buffer PP (12.5% Glycerin, 3% SDS, 125 mM Tris (PH=6.8), 1% of protease inhibitor, and 1% of phosphatase inhibitor) for 30 min on ice followed by ultrasonification for 6-8 times on ice and then centrifuged at 16000 g at 4°C for 15 min. The supernatants were transferred into another tube and kept at -80°C.

Measurement of protein concentration

The protein concentration was measured by the Micro-BCA^{TM} Protein assay kit. A series of standard solutions (0, 1, 3, 5, 10, 20 and 40 µg/ml) were prepared by graduate dilution of standard albumin in working solution (a mixture of 48% reagent B, 2% of reagent C and 50% reagent A). Sample (3 µl) was then mixed with 500 µl of working solution and incubated for 60 min at 60°C. After cooling down to room temperature, 100 µl of each reaction was taken to measure the absorbance at 570 nm. The concentration of each sample was calculated according to the BCA standard calibration curve.

Gel electrophoresis

The separation gels were prepared according to the protocol as described before following 1 h polymerization. The collecting gel was then added on top of the separating gel and incubated for another 1 h. The protein samples were mixed with loading buffer (1:4, v/v) and denatured at 95°C for 5 min. 20-25 µg protein from each sample was loaded on the gel and run at 20 mA, 150 V for about 45 min.

Blotting

After electrophoresis, the gel was washed in the blotting buffer. A nitrocellulose transfer membrane was pre-wetted in the blotting buffer. For blotting, the gel containing proteins was laid directly on a sheet of pre-wetted nitrocellulose membrane, which was sandwiched between two pre-wetted filter papers and two pre-wetted sponges. Afterward, the proteins were transferred from the gel onto the nitrocellulose membrane at 300 mA, 150 V for 1 h. The transferred protein was examined by staining the membrane with ponceau S to make sure the protein was completely transferred. The membrane was thereafter washed with tris buffered saline (TBS) and incubated with 5% of non-fat dry

milk in TBS at room temperature for 2 h to block the unspecific bindings. The blots were then incubated with different primary antibodies overnight at 4°C. The following primary antibodies were used: rabbit anti-PDCD10 (1:400) and rabbit anti-GAPDH (each 1:1000 dilution). After the incubation with the corresponding HRP-conjugated secondary antibody (1:2000) at room temperature for 1 h, the signal was produced by using ECL solution. To semi-quantify the blot, the IOD of each band was measured using Image J software. The IOD ratio of the target protein to housekeeping protein GAPDH was calculated and normalized to the percentage of the control.

2.2.6 Enzyme-linked immunosorbent assay (ELISA)

The proteins were extracted from the cell pellets with the treatment of 10 nM NVP and the tumor tissue from the animal study. The level of phosphor-EphB4 (p-EphB4), reflecting the kinase activity of EphB4, was measured according to the manufacture's instruction by using an ELISA kit.

2.2.7 Protein array

Human angiogenesis array was performed to explore the potential mechanism mediated the phenotype change of ECs after treatment of CM from the PDCD10 knockdown GBM cells.

Medium collection

A total of 1.6×10^6 EV- and shPDCD10-U87cells were plated onto the 100 mm PD and incubated until the confluence reached 80%. The medium was refreshed and the cells were continuously cultured or 2 days. The media was collected, centrifuged shortly, and transferred into a new tube, which was stored at -80°C until use.

Protein array assay

Protein array was performed by using a human angiogenesis array kit containing 2 membranes according to the instruction. Briefly, each membrane was identically pre-coated with antibodies against 55 different angiogenic proteins (listed in Table 2), and each protein was detected in duplicate. The two membranes were incubated with a blocking buffer at room temperature for 2 h, following by incubation with cultured media

collected from EV- or shPDCD10-U87 cells (1 ml), array buffer-5 (0.5 ml) and reconstituted detection antibody cocktail (15 µl) at 4°C overnight. After the incubation of the membranes with 2.0 ml of diluted streptavidin-HRP at room temperature for 30 min, the signal was detected by the ECL solution. The IOD of each dot in CM was measured using Image J software. Each protein was detected in duplicated form. The target protein was then presented as fold of the control.

Table 2 List of soluble factors in protein array

Target proteins detected by the protein array		
Activin A	FGF-7 (KGF)	PDGF-AB/PDGF-BB
ADAMTS-1	GDNF	Persephin
Angiogenin (ANG)	GM-CSF	Platelet Factor 4 (PF4)
Angiopoietin-1 (Ang-1)	HB-EGF	PlGF
Angiopoietin-2 (Ang-2)	HGF	Prolactin
Angiostatin/Plasminogen	IGFBP-1	Serpin B5 Maspin
Amphiregulin (AR)	IGFBP-2	Serpin E1 PAI-1
Artemin	IGFBP-3	Serpin F1 PEDF
Coagulation Factor III	IL-1β (IL-1F2)	PD-ECGF
CXCL16	IL-8 (CXCL8)	TIMP-1
DPPIV (CD26)	LAP (TGF-β1)	TIMP-4
EGF	Leptin	Thrombospondin-1 TSP-1
EG-VEGF (PK1)	MCP-1 (CCL2)	Thrombospondin-2 TSP-2
Endoglin (CD105)	MIP-1α (CCL3)	uPA
Endostatin/Collagen XVIII	MMP-8	Vasohibin
Endothelin-1 (ET-1)	MMP-9	VEGF
FGF acidic (FGF-1)	NRG1-β1 (HRG1-	VEGF-C
FGF basic (FGF-2)	Pentraxin 3 (PTX3)	Reference Spots
FGF-4	PDGF-AA	Negative control

2.2.8 Human GBM xenograft model

Female nude mice (4-6 weeks old) were obtained from the animal center of Medical College, Duisburg-Essen University and housed in a specific pathogen-free animal

environment. For each plug implantation, 1×10^6 EV- and shPDCD10-U87cells were harvested and suspended in 200 µl of matrigel and fibrinogen (final concentration 2 mg/ml) containing VEGF and bFGF (final concentration 500 ng/ml each). After mixing with thrombin (final concentration 0.625 U/ml), the plugs were subcutaneously implanted into the flank of the mice as described in the previous publication. To maintain the stable knockdown of PDCD10 *in vivo*, 2 mg/mL doxycycline and 1% sucrose was added to the drinking water. The xenograft tumors were removed from the mice for further studies 21 days after implantation. To investigate whether inhibition of EphB4 could rescue shPDCD10-induced tumor growth, the mice implanted with shPDCD10-U87 were treated with NVP (8 mg/kg, i.g.) every two days beginning on the sixth day after implantation. The control mice received the same amount of solvent without treatment (the solvent containing 10% v/v 1-methyl-2-pyrrolidone (Sigma, Munich, Germany) and 90% v/v polyethylene glycol 300 (Sigma, Munich, Germany)). The tumor size was measured twice a week by using a caliper. The tumor volume (VT) was calculated according to a formula: VT= $\pi/6$ x larger diameter x (smaller diameter)^2. The xenograft tumors were removed from the mice 21 days after implantation for further studies. The tumor masses were weighed and recorded.

Evaluation of proliferation and neoangiogenesis in xenograft tumor sections

The proliferation of the cells in slices was evaluated by staining using mouse anti-Ki67 (1:200). The micro-vascular like structures of slices were detected by staining of mouse anti-CD31 (1:40). The images were acquired using a fluorescence microscope (Axio Imager M2, Zeiss, Oberkochen, Germany).

2.2.9 Statistical analysis

Statistical analysis was performed using the WinSTAT program. Results among 3 groups were analyzed by the *ANOVA* test and the Student *t*-test was applied to analyze the data between 2 groups. A *P* value less than 0.05 was considered statistically significant. All data were presented as Mean±SD.

3. Results

3.1 Confirmation of PDCD10 knockdown and activation of EphB4 in PDCD10 knockdown GBM cells

The morphology of shPDCD10 and EV-GBM cells was presented in Figure 1. To investigate the knockdown efficiency of PDCD10 and the effect of shPDCD10 on EphB4 expression and kinase activity in GBM cells, the level of PDCD10 and EphB4 mRNA, protein and p-EphB4 were studied in two different GBM cell lines in which PDCD10 were knocked down by shRNA transduction. As detected by RT^2-PCR, the expression of PDCD10 in shPDCD10-U87 cells and shPDCD10-T98g cells was reduced to 37 % and 33 % of the control, respectively (both $P<0.001$), concomitantly accompanied by a 2.7-fold ($P<0.05$) and a 3.1-fold ($P<0.01$) up-regulation of EphB4 mRNA (Figure 2A). ELISA for p-EphB4, reflecting the kinase activity of EphB4, showed a 280 % ($P<0.01$) and a 150% ($P<0.05$) increase in the level of p-EphB4 in shPDCD10-U87 and shPDCD10-T98g cells in comparison to the controls, respectively (Figure 2B). Furthermore, PDCD10 knockdown-mediated activation of EphB4 was abolished by the specific EphB4 kinase inhibitor NVP-BHG712 (NVP) in both U87- and T98g cells. Western blot confirmed significant downregulation of PDCD10 protein expression in shPDCD10-U87 and shPDCD10-T98G cells (both $P<0.001$), accompanied by an activation of Erk1/2 but not Akt (Figure 2C; left panel). The semiquantitative analysis showed a 2.9-fold ($P<0.05$) and a 2.1-fold ($P<0.05$) up-regulation of EphB4 and p-Erk1/2 in shPDCD10-U87 cells, respectively; a 1.5-fold ($P<0.05$) and a 2.2-fold ($P<0.05$) up-regulation of EphB4 and p-Erk1/2 in shPDCD10-T98g cells were detected (Figure 2C; right panel). NVP treatment partially reversed the activation of Erk1/2 derived by PDCD10 knockdown. The upregulated EphB4 protein level in shPDCD10 was not influenced by NVP (Figure 2C), which is however not surprising as NVP selectively inhibits autophosphorylation of EphB4, but does not influence the EphB4 gene transcription or protein translation processes.

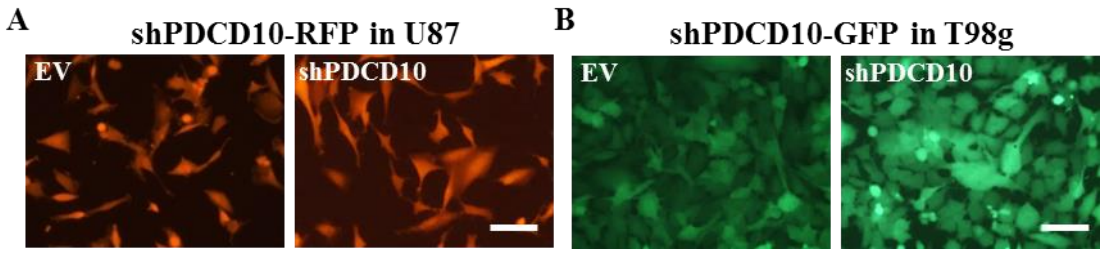

Figure 1 Successful transduction of PDCD10 in GBM cells

The knockdown of PDCD10 was done by lentiviral transduction of shRNA specifically targeting PDCD10 and an empty vector using two different packaging systems. **A** Transduced U87 cell expressing red fluorescence protein (RFP). **B** Transduced T98g cell expressing green fluorescent protein (GFP). The representative pictures are shown.

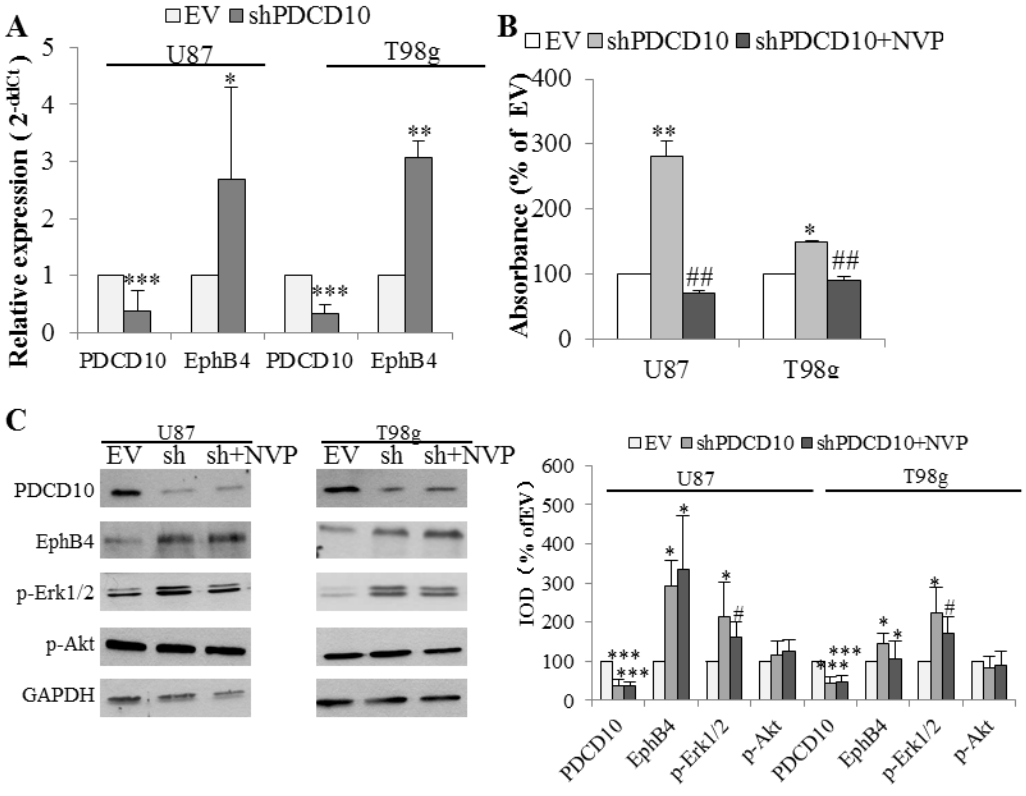

Figure 2 Knockdown of PDCD10 increased the expression and the kinase activity of EphB4 in GBM cells, which was reversed by the treatment with the specific kinase inhibitor of EphB4 (NVP)

PDCD10 was knocked down in U87 or T98g cells by lentiviral shRNA transduction. **A**

RT^2-PCR demonstrated a significant downregulation of PDCD10 mRNA and upregulation of EphB4 mRNA in PDCD10 knockdown (shPDCD10) U87 and T98g cells in comparison to EV-transduced cells. **B** ELISA demonstrated that knockdown of PDCD10 elevated the level of p-EphB4, reflecting the activity of EphB4, which was reversed upon the treatment with NVP (10 nM), a specific EphB4 kinase inhibitor. **C** Western blot revealed that knockdown of PDCD10 increased the EphB4 protein expression and activated Erk1/2 but not Akt in GBM cells (left panel). The activation of Erk1/2 mediated by PDCD10 knockdown was partially reversed by the treatment of NVP. Semiquantification of the blots was performed measuring the integrated optical density (IOD) of the blots normalized to the IOD of housekeeping protein GAPDH (right panel). All data presented in A-D were representative of at least three independent experiments. *P<0.05, **P<0.01 and ***P<0.001, compared with EV; #P<0.05, ##P<0.01, ###P<0.001, compared with shPDCD10.

3.2 Knockdown of PDCD10 activated GBM cells, which was rescued by the specific kinase inhibitor of EphB4 (NVP-BHG712)

3.2.1 Knockdown of PDCD10 promoted proliferation of T98g cells, which was reversed by NVP-BHG712 treatment

To evaluate the phenotype change after knockdown of PDCD10 in GBM cells, the proliferation of T98g cells was studied. As shown in Figure 3, the loss of PDCD10 significantly stimulated a 97% (P<0.001) increase in the proliferation of T98g cells. However, this effect was reversed by the treatment of 25 nM NVP-BHG712 (NVP) for 24 h.

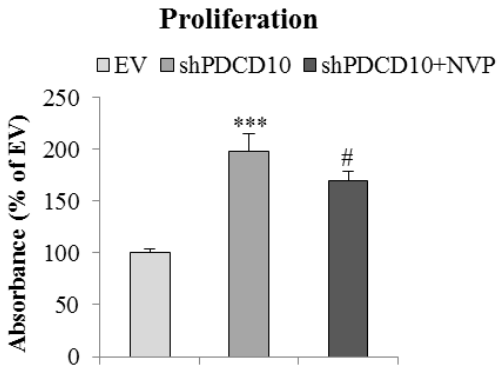

Figure 3 Knockdown of PDCD10 promoted proliferation of T98g cells, which was rescued by the treatment of NVP

T98g or U87 cells (2000/well) were seeded into 96-well plate and the proliferation was measured 24 hours after seeding by WST-1 assay at 450 nm. All data presented were representative of at least three independent experiments. ***P<0.001, compared with EV; #P<0.05, compared with shPDCD10.

3.2.2 Knockdown of PDCD10 enhanced adhesion of T98g cells, which was suppressed by the treatment of NVP-BHG712

For the GBM cell adhesion study, knockdown of PDCD10 in T98g cells enhanced adhesion ability (P<0.001) compared to the control (Figure 4), which was significantly inhibited by the treatment with NVP (25 nM).

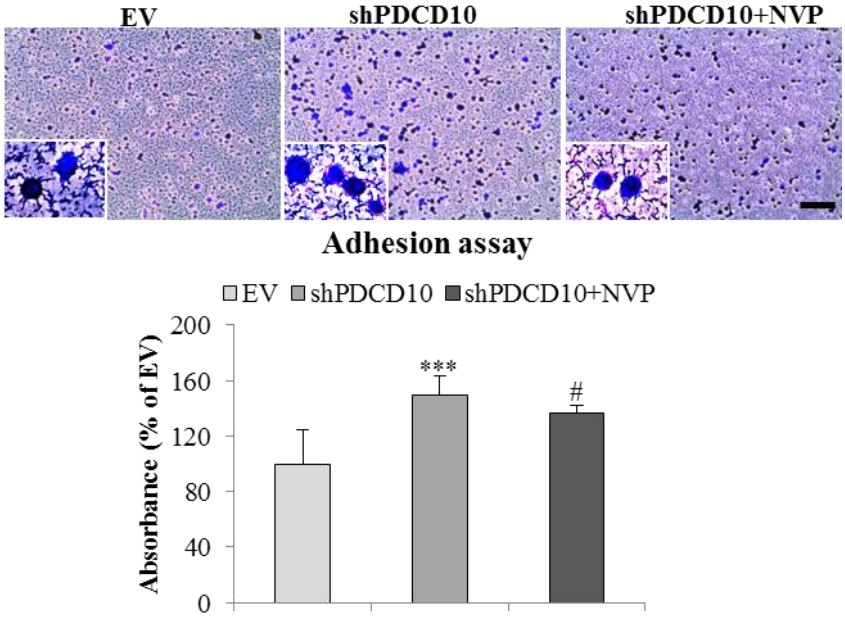

Figure 4 Knockdown of PDCD10 enhanced adhesion of T98g cells, which was suppressed by the treatment of NVP

Cell adhesion was measured 90 minutes after seeding cells in a 96-well plate precoated with Matrigel. The adherent cells were stained by crystal-violet staining (0.5%), and lysis by 1% SDS, followed by measuring the absorbance at 550 nm. **Upper panel:** Representative pictures of crystal-violet staining of at least three independent experiments. **Lower panel:** Quantification of absorbance of adhesion cells. ***P<0.001, compared with EV; #P<0.05, compared with shPDCD10. Scale bar: 100 μm.

3.2.3 Knockdown of PDCD10 activated migration of T98g cells, which was inhibited by the treatment of NVP-BHG712

After the knockdown of PDCD10, the migration of GBM cells was evaluated by two different methods, including scratch assay and spheroid migration assay. The migration activity of T98g cells remarkably increased after knockdown of PDCD10, which was confirmed in the scratch assay (P<0.01) (Figure 5) and spheroid migration assay (P<0.01) (Figure 5). NVP (10 or 25 nM) could suppress this effect caused by the loss of PDCD10.

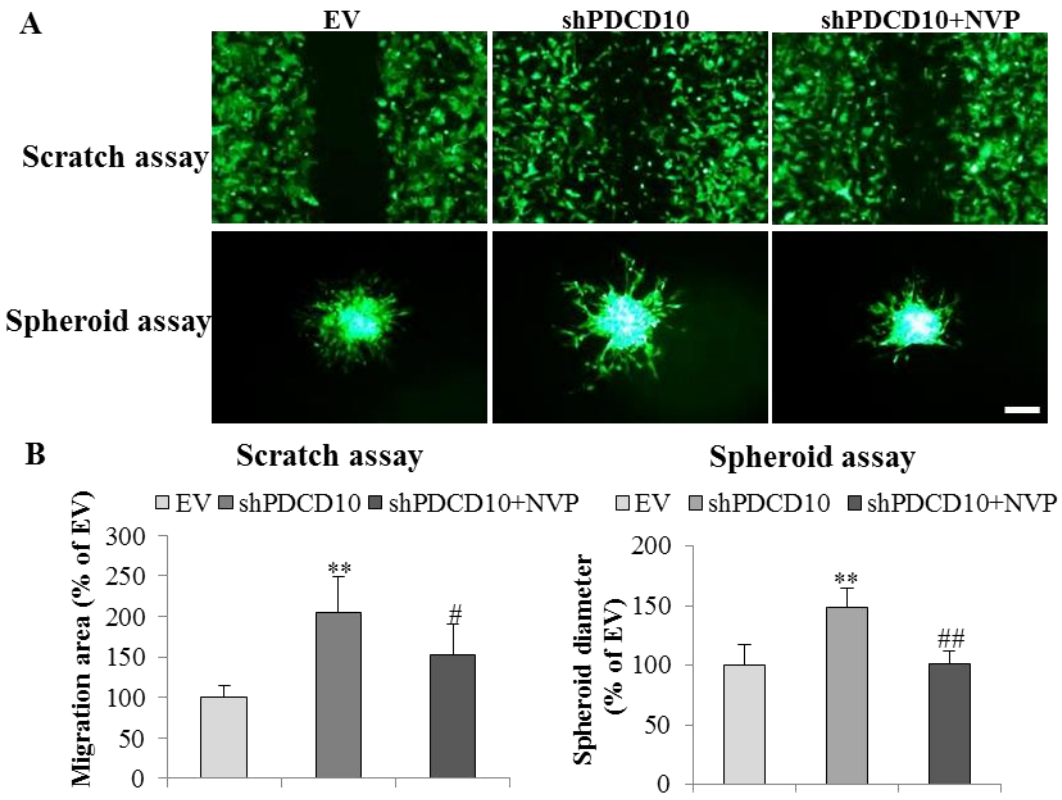

Figure 5 Knockdown of PDCD10 activated migration of T98g cells, which was inhibited by the treatment of NVP

A Scratch assay of T98g transduced cells. **Upper panel:** Representative pictures of the scratch assay for T98g transduced cells; **lower panel:** Representative pictures of spheroid migration assay for T98g transduced cells 48h after reseeding. **B** Quantification of migrated area (for scratch assay) or spheroid diameters (for spheroid migration assay) of T98g transduced cells. For the scratch assay, 3×10^5 cells were plated into 35 mm plate. When the confluence of cells reached about 90 %, 2 or 3 scratch lines were made with a 100 µl tip across the marked lines, followed by washing twice with the medium and refreshing the medium with or without 10 nM NVP. The photos were recorded immediately at 0 h and 24 h after scratching. The cell-free area was quantified by using Image J software and the migrated area reflexes the closed area when of the area at 0 h time point substrate the area measured at 24 h after scratching. Scale bar: 200 µm. For spheroid migration assay, 1.0 x 10^3 T98g transduced cells were suspended in a medium containing 20% methylcellulose and plated into U shape 96-well plates to generate the

spheroids. After incubation overnight, the formation and quality of the spheroids were evaluated under 5 magnification. Nicely formed spheroids (round and regular) were carefully picked up and reseeded into a flat shape 96-well plate precoated with matrigel (0.5 mg/ml). 100 µl medium with or without 25 nM NVP were added into each well. The spheroids were then photographed by an inverse fluorescence microscopy and the spheroid diameter was recorded at 48 h after the incubation. Scale bar: 100 µm. Each experiment was performed at least three times. **P<0.01, compared to EV and #P<0.05, ##P<0.01 compared to shPDCD10.

3.2.4 Knockdown of PDCD10 stimulated T98g cell invasion, which was hindered by the treatment of NVP-BHG712

Invasion contributes to tumor progression, especially in GBM. After the knockdown of PDCD10, an enhanced invasion of T98g was also observed. The invaded cells increased by 127% (P<0.05) compared to the control (Figure 6) and the treatment with NVP significantly inhibited the activated GBM cell invasion resulted from PDCD10 knockdown.

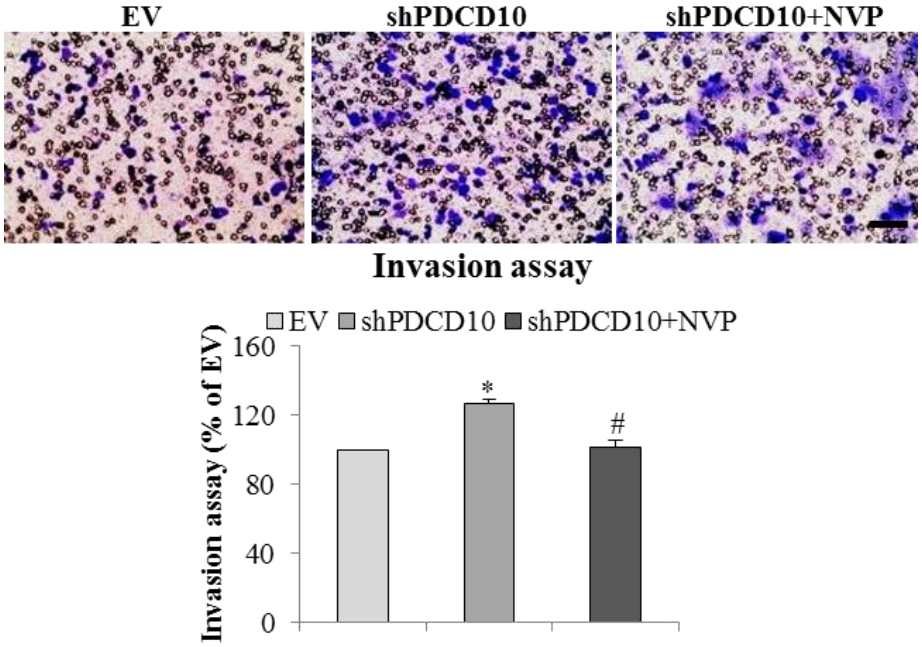

Figure 6 Knockdown of PDCD10 stimulated invasion of T98g cells, which was

hindered by the treatment of NVP

A Invasion assay after PDCD10 knockdown for T98g cells. **B** Quantification of invaded cells. After starvation of the cells overnight, cells were plated into 24-well transwell plates coated with matrigel (8 μm-pore size) in serum-free medium with or without 25 nM NVP. Invasive cells were stained by crystal-violet and the absorbance was measured by a plate reader at 550 nm. Scale bar: 50 μm. The experiments were independently repeated at least twice, respectively. *P<0.05, compared to EV and #P<0.05, compared to shPDCD10.

3.3 Conditioned medium from shPDCD10 GBM cells triggered endothelial cells (ECs)

3.3.1 Conditioned medium from shPDCD10 T98g cells stimulated HUVECs growth

Indirect co-culture was applied to investigate the growth of HUVECs in the conditioned medium. As shown in Figure 7, the conditioned medium from shPDCD10 T98g cells could promote the growth of HUVECs.

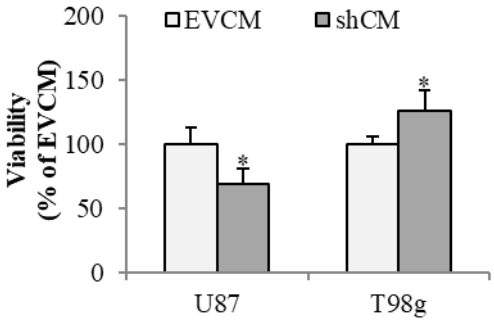

Figure 7 Conditioned medium from shPDCD10 T98g cells stimulated HUVECs growth

HUVECs (4000/well) were plated into 96-well plate. After overnight incubation, the indicated CM (The EVCM was composed of the 50% collected media from EV-U87 or EV-T98g cells and 50% of ECGM with supplements, and the shCM was made up of 50% collected media from shPDCD10-U87 or shPDCD10-T98g cells and 50% of ECGM with supplements.) was refreshed followed by 24 h incubation. MTT was added to the culture and incubated for 3 h, thereafter, 150 μl of MTT solvent was added to each well to

dissolve the MTT formazan and the plate was incubated on an orbital shaker for 15 min at room temperature. The absorbance was detected at 590 nm in a plate reader. All data presented were representative of at least three independent experiments. *P<0.05, compare to EVCM.

3.3.2 Conditioned medium from shPDCD10 GBM cells promoted HUVECs adhesion

For adhesion study, CM from shPDCD10 U87 and T98g cells enhanced the adhesion of HUVECs (P<0.01 in U87 CM and P<0.05 in T98g CM) compared to their corresponding controls (Figure 8)

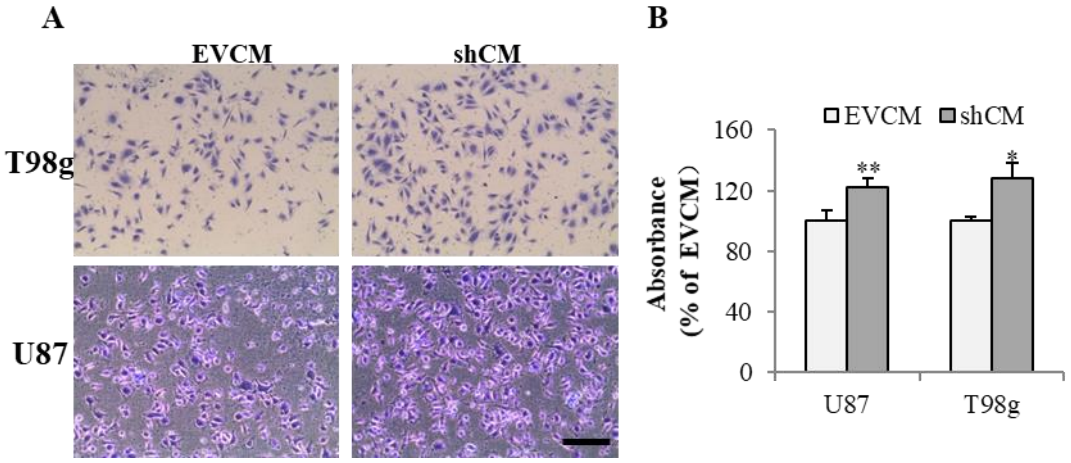

Figure 8 CM from PDCD10 knockdown GBM cells promoted HUVECs adhesion

A A total of 1×10^4 HUVECs were suspended in indicated CM (The EVCM and shCM were defined as before.) and seed gelatin precoated 96 well plates. The adherent cells after 90 min were stained by crystal-violet staining (0.5%), and lysis by 1% SDS, followed by measuring the absorbance at 550 nm. **A** Representative picture of crystal-violet staining of at least three independent experiments. **B** Quantification of absorbance of adhesion cells. *P<0.05 and **P<0.01, compare to EVCM.

3.3.3 Conditioned medium from shPDCD10 GBM cells enhanced HUVECs migration

Two different methods, namely scratch assay and spheroid migration assay were applied

to investigate the motility of HUVECs treated with CM in this study. The migration activity of HUVECs after treated with CM from both shPDCD10-U87 and -T98g cells remarkably increased in the scratch assay ($P<0.01$ for U87 CM and $P<0.05$ for T98g CM) (Figure 9). The enhanced migration activity was also observed in the spheroid assay for shPDCD10-U87 CM ($P<0.01$) and shPDCD10-T98g CM ($P<0.05$) (Figure 10).

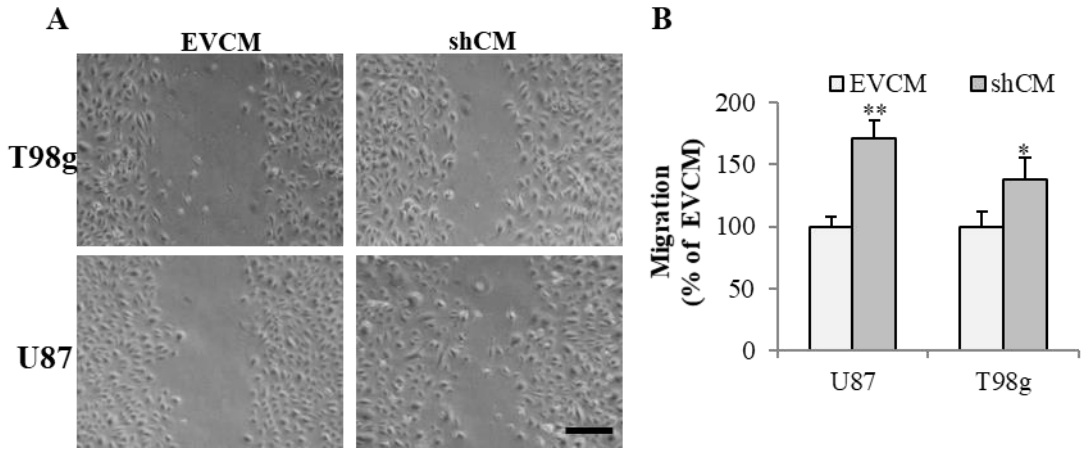

Figure 9 CM from shPDCD10-GBM cells enhanced HUVECs migration

A Representative picture of the scratch assay for HUVECs treated with U87 and T98g CM (The EVCM and shCM were defined as before.) 12 h after scratch; **B** Quantification of the migrated area of HUVECs. HUVECs (3×10^5/PD) were plated into 35 mm PD. When the confluence of cells reached about 90%, 2 or 3 scratch lines were made with a 100 µl tip across the marked lines, followed by washing twice with the medium and refreshing the indicated conditioned medium. The photos were recorded immediately as 0 h and 12 h after scratching. The cell-free area was quantified by using Image J software and the migrated area reflexes the closed area when of the area at 0 h time point substrate the area measured at 12 h after scratching. *$P<0.05$ and **$P<0.01$, compared to EVCM. Scale bar: 200 µm.

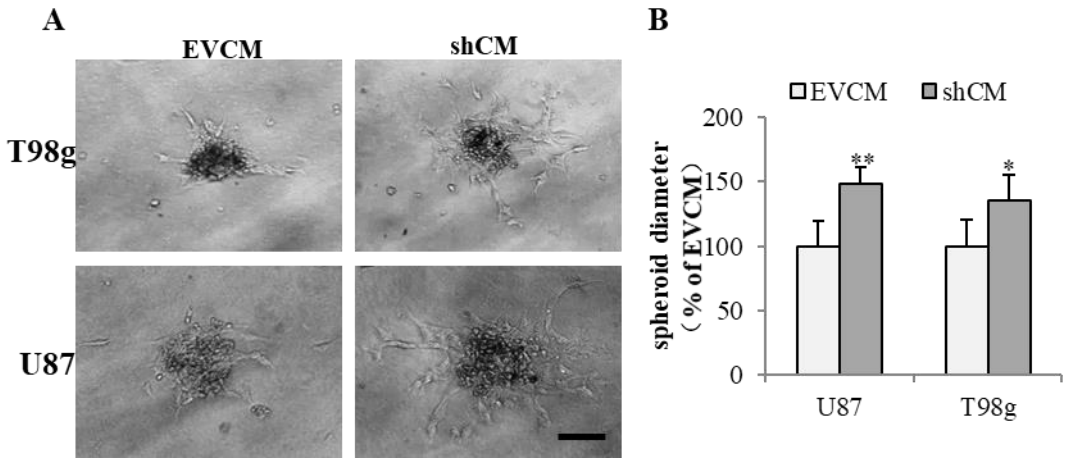

Figure 10 CM from shPDCD10-GBM cells stimulated HUVECs migration

A Representative pictures of spheroid migration assay for HUVECs treated with U87 and T98g CM (The EVCM and shCM were defined as before.) 24 h after reseeding. **B** Quantification of the diameter of HUVECs spheroids. A total number of 500 HUVECs cells were suspended in a medium containing 20% methylcellulose and plated into U shape 96-well plates to generate the spheroids. After incubation overnight, the formation and quality of the spheroids were evaluated under 5 magnification. Nicely formed spheroids (round and regular) were carefully picked up and reseeded into a flat shape 96-well plate precoated with matrigel (0.5 mg/ml). 100 µl indicated conditioned medium was added into each well. The spheroids were then photographed by an inverse fluorescence microscopy and the spheroid diameter was recorded at 24 h after the incubation. Scale bar: 100 µm. *P<0.05 and **P<0.01, compared to EVCM.

3.4 Knockdown of PDCD10 promoted tumor progression *in vivo*, which was suppressed by the treatment of NVP-BHG712

3.4.1 Knockdown of PDCD10 promoted tumor progression *in vivo*, which was suppressed by the treatment of NVP-BHG712

ShPDCD10 or EV U87 cells were subcutaneously implanted into the flank of nude mice, and the tumors were resected and weighed before being analyzed by RT^2-PCR, Western blot, ELISA and tissue staining. RT^2-PCR (Figure 11Ba) and Western blot (Figure 11Bb)

confirmed a stable knockdown of PDCD10 in tumors derived from transplanted shPDCD10-U87 cells. Part of the protein lysate (produced for Western blot) was used to perform ELISA for p-EphB4. We found a drastically increased level of p-EphB4 in the PDCD10-knockdown tumors compared to the controls (Figure 11C). The NVP treatment completely reversed the upregulation of p-EphB4 in xenograft tumors of the PDCD10-knockdown mice. Consequently, the tumor progression was significantly faster in the shPDCD10-mice than that in the controls as inspected from day 7 to day 21 after implantation (Figure 11D). The tumor mass was weighed at the end of the experiment (21 days after implantation) was 2.3-fold in the shPDCD10-mice than that in the controls ($P<0.05$) (Figure 11E). More importantly, the treatment with NVP not only abolished PDCD10-knockdown-mediated activation of EphB4 (Figure 11C), but also suppressed the aggressive tumor progression and rapid growth in shPDCD10 mice (Figure 11D, E).

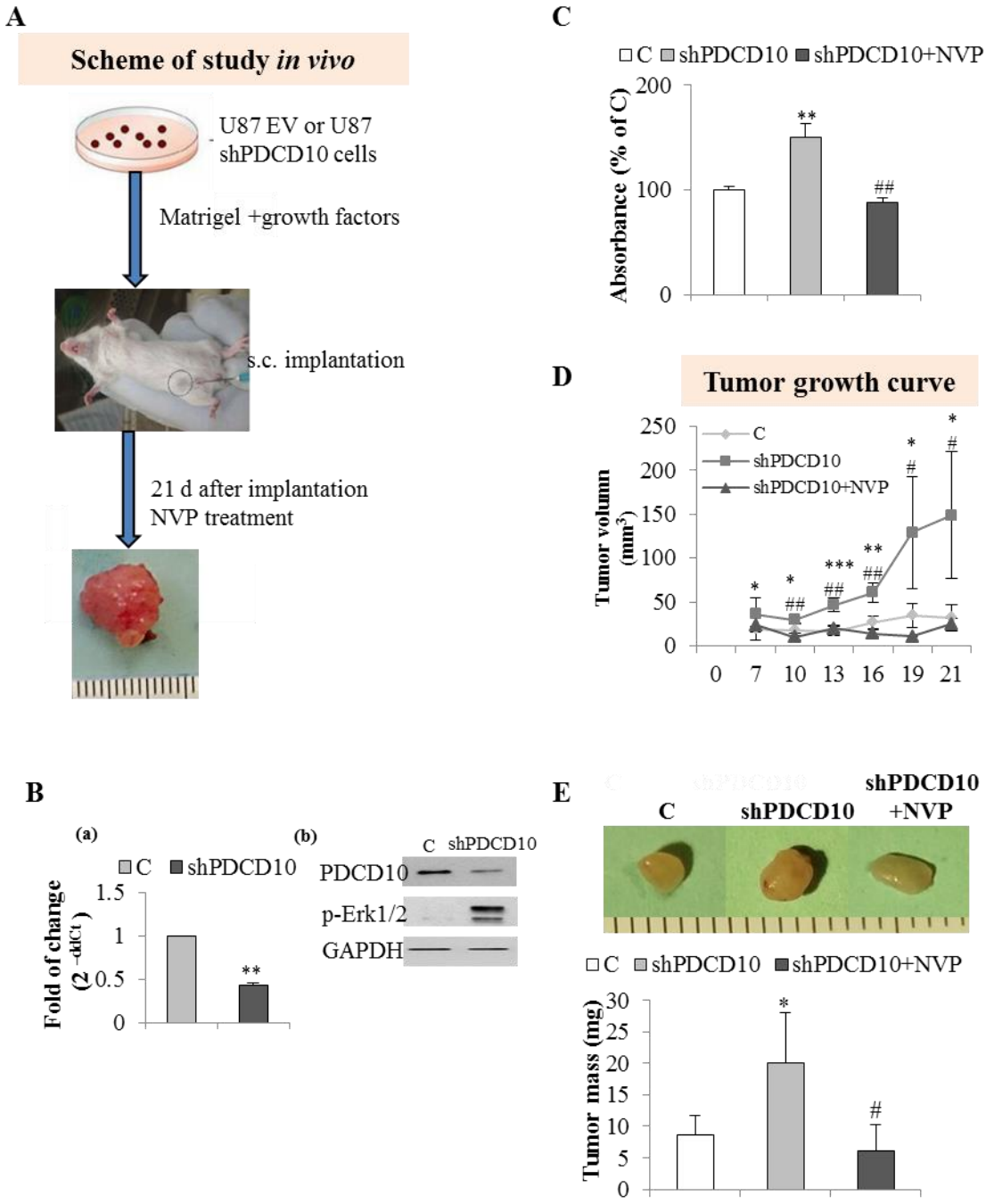

Figure 11 Knockdown of PDCD10 promoted tumor progression *in vivo*, which was suppressed by the treatment of EphB4 kinase inhibitor NVP

A The scheme of study in vivo. A total of 1 million shPDCD10-transduced U87 cells with matrigel and growth factors were subcutaneously implanted into the flank of nude mice. To maintain the stable knockdown of PDCD10 *in vivo*, 2 mg/ml doxycycline (dox) and 1% sucrose were added to the drinking water. For the control group (C), transduced cells

were cultured in a dox-free medium *in vitro* and the drinking water for the control mice contained only 1% sucrose after implantation *in vivo*. To investigate whether inhibition of EphB4 could rescue shPDCD10-induced tumor growth, the mice implanted with shPDCD10-U87 were treated with NVP (8 mg/kg, i.g.) every two days beginning on the sixth day after implantation. The control mice received the same amount of solvent without treatment (the solvent containing 10% v/v 1-methyl-2-pyrrolidone (Sigma, Munich, Germany) and 90% v/v polyethylene glycol 300 (Sigma, Munich, Germany)). The xenograft tumors were removed from the mice after 21 days of implantation. n=7 for each group. **B** Expression of PDCD10 in resected tumors at mRNA (a) and protein levels (b) determined by RT^2-PCR and Western blot, respectively. **C** ELISA for p-EphB4 demonstrated the activation of EphB4 in PDCD10-knockdown tumors, which was completely reversed after treatment with NVP. **D** The tumor growth curve revealed a significantly faster tumor progression in PDCD10-knockdown tumors and a marked tumor growth inhibition by the treatment with NVP. **E** NVP treatment reduced significantly the tumor mass compared to that from PDCD10-knockdown mice. Upper panel: the representative images show the tumors from control, shPDCD10, and NVP-treated shPDCD10-mice, respectively. Lower panel: statistical analysis, *P<0.05, **P<0.01, ***P<0.001, compared to control; #P<0.05, ##P<0.01, compared to shPDCD10.

3.4.2 Knockdown of PDCD10 activated the proliferation of shPDCD10 U87 cells *in vivo,* which was inhibited by the treatment of NVP-BHG712

Cell proliferation in xenograft tumors was evaluated by immunochemistry staining of Ki67 on the sections. It's noteworthy that Ki67 immunohistochemistry staining showed extensive Ki67-positive cells on the section from shPDCD10-mice than that from the control (P<0.05, Figure 12), however, the Ki67-positive cells were much fewer in the NVP treatment group compared to that from shPDCD10-mice.

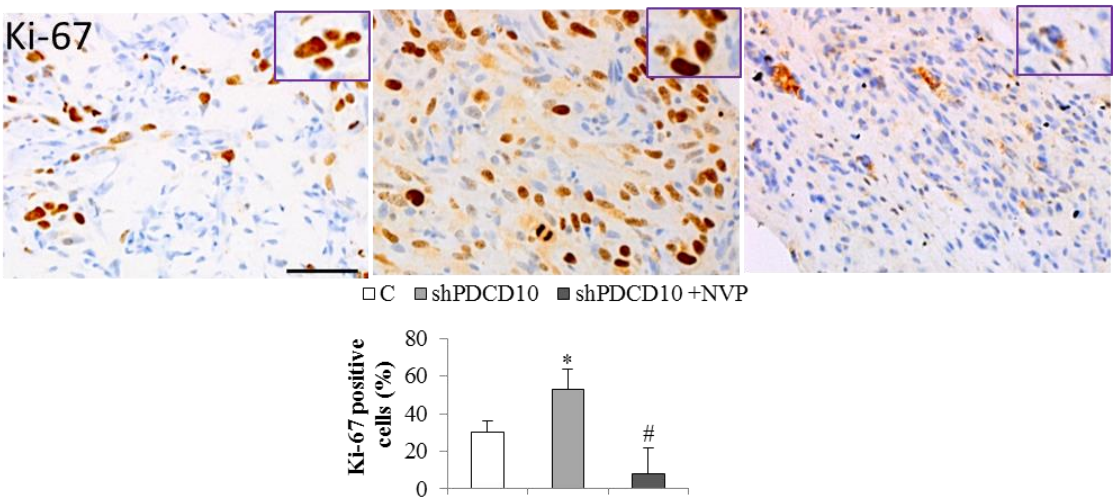

Figure 12 Knockdown of PDCD10 activated proliferation of U87 cells *in vivo,* which was inhibited by NVP

Upper panel: Representative photos showed the proliferating cells (Ki67 positive cells) in the tumor section. Scale bar: 50 μm. **Lower panel:** Quantification of Ki67-positive cells in tumor sections indicated that more extensive Ki67-positive cells on the section from shPDCD10-mice than that from the control. *P<0.05, compared to C and #P<0.05, compared to shPDCD10.

3.4.3 Knockdown of PDCD10 promoted the neo-angiogenesis of shPDCD10 U87 cells *in vivo,* which was rescued by NVP-BHG712

To determine the role of PDCD10 on neo-angiogenesis *in vivo*, H&E staining and CD31 immunochemistry staining were performed on the sections from the tumors formed by shPDCD10 U87 and control cells. H&E staining revealed the histological features of the xenograft tumors comprising more micro-vascular like structures that often contained blood cells (upper panel, Figure 13), indicating a functional vascular network in xenograft tumors. CD31-immunohistochemistry staining demonstrated that the deletion of PDCD10 in GBM cells led to the formation of micro-vascular like structures in xenograft (P<0.05) (lower panel, Figure 13). As a consequence, the tumor growth rate was significantly faster in shPDCD10-mice than in the control mice as inspected from days

10–21 days after implantation (Figure 11D). On day 21 after implantation, the tumor mass in the shPDCD10-mice was 2.3-fold larger than that in the controls (P<0.05) (Figure 11E). However, this effect caused by the loss of PDCD10 was hindered by the treatment of NVP.

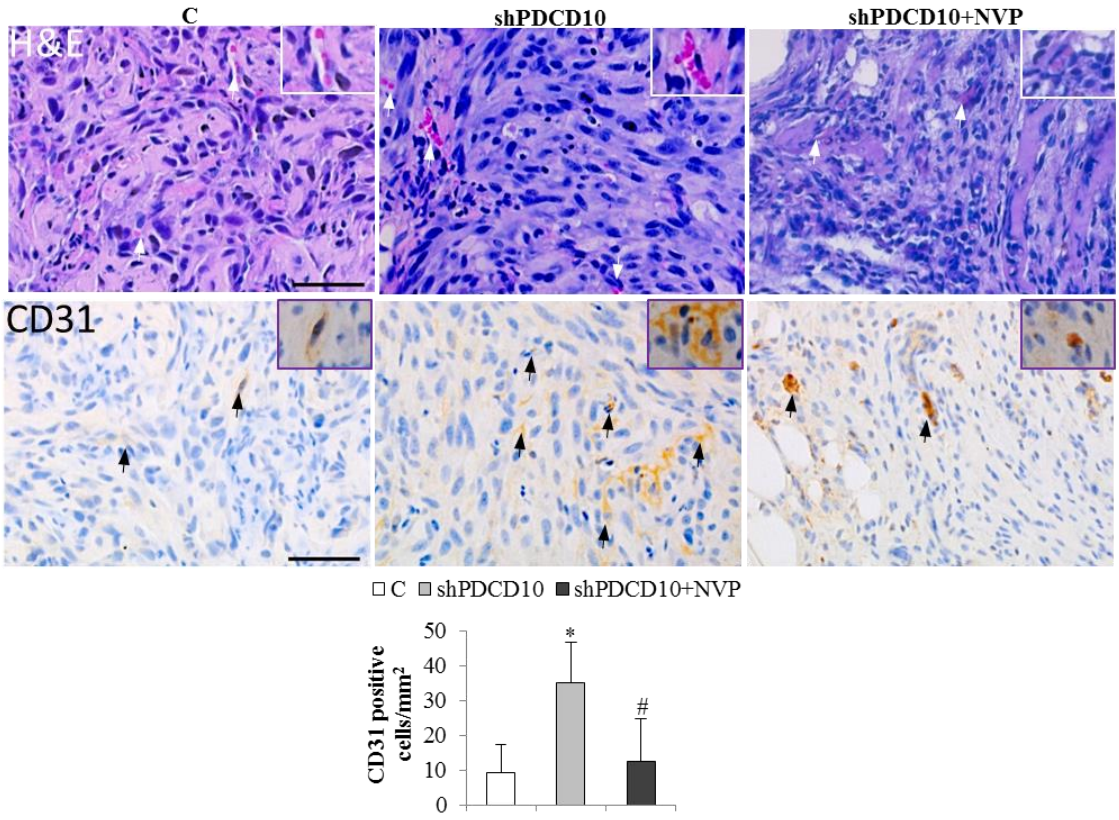

Figure 13 Knockdown of PDCD10 promoted neo-angiogenesis of U87 cells *in vivo*, which was rescued by NVP

A Representative photo showed the histological morphology (H&E staining) and vessel-like structure (CD31-positive structure) in the tumor sections. Scale bar: 50 μm. **B** Quantification of micro-vascular like structures per mm^2 indicated more vascular like structures could be observed in shPDCD10 xenograft tumors. *P<0.05, compared to C and #P<0.05, compared to shPDCD10.

3.5 Knockdown of PDCD10 in GBM cells stimulated the release of pro-angiogenic factors

To explore the mechanism of conditioned medium (CM) from loss of tumor-originated

PDCD10 in GBM cells triggering ECs, we performed a protein array of 55 soluble factors in CM from U87 EV and shPDCD10 culture media. Before the experiment, the efficiency of PDCD10 knockdown in U87 cells was confirmed. The dot-blots reflecting the protein expression were shown in Figure 14A. Semi-quantification of the blots revealed that 19 of 55 target proteins showed 1.5-fold upregulation in the shPDCD10 group, which were Angiogenin, ADAMTS-1, Amphiregulin, Artemin, Coagulation Factor III, CXCL16, Endoglin, FGF acidic, FGF-4, GDNF, HB-EGF, HGF, Leptin, CCL2, CCL3, PDGF-AB/BB, TSP-1, TSP-2 and Vasohibin (Figure 14B). Among these factors, 8 soluble factors were upregulated more than 2 folds, and the most significant upregulation is Angiogenin (Figure 14C).

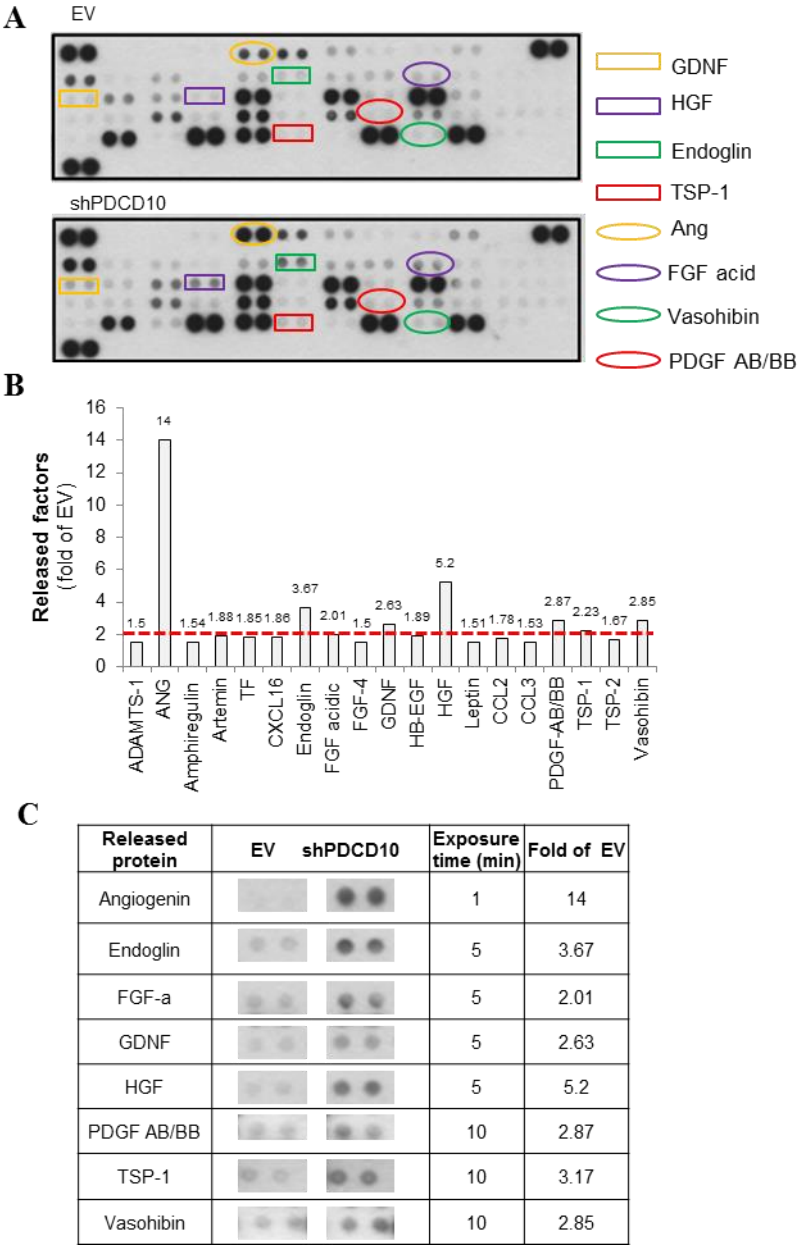

C

Released protein	EV shPDCD10	Exposure time (min)	Fold of EV
Angiogenin		1	14
Endoglin		5	3.67
FGF-a		5	2.01
GDNF		5	2.63
HGF		5	5.2
PDGF AB/BB		10	2.87
TSP-1		10	3.17
Vasohibin		10	2.85

Figure 14 Loss of PDCD10 in GBM cells stimulated the release of proangiogenic factors

Soluble proangiogenic factors of conditioned medium (CM) from U87 cells were detected by the human angiogenesis antibody array. **A** Dot-blots on X-ray film (5 min exposure). **B** Semi-quantification of the blots showed 19 upregulated proteins (>1.5-fold of EV) among 55 detected proteins. **C** Summary of 8 proteins that were upregulated more than 2-fold in shPDCD10 cells in comparison with EV control.

4. Discussion

As described in the introduction part, PDCD10 is a universally expressed adaptor protein and involves in the vasculogenesis and angiogenesis (Fischer et al, 2013), cell apoptosis, autophagy senescence (Draheim et al, 2014; Marchi et al, 2015) and chemotherapy-resistance (Urfali-Mamatoglu et al, 2018; Zhang et al, 2016). However, the understanding of the function of PDCD10 is mainly from ECs since it has been identified to be one cause of familial CCM, one of the most common vascular malformations in the central nervous system (CNS), thereafter, it has been intensively studied in the vascular endothelial system throughout the past decade to explore the underlying mechanism (You et al, 2013; You et al, 2017; Zhu et al, 2010). Nowadays, preliminary evidence indicates that PDCD10 might be involved in the progression of the tumor: firstly, as a pleiotropic protein, PDCD10 could interact with a variety of signaling proteins, thereby regulating multiple functions, including migration, angiogenesis, apoptosis and senescence, oxidative metabolism and Golgi complex polarization (Draheim et al, 2014; Fidalgo et al, 2010; Madsen et al, 2015; Schleider et al, 2011; Zheng et al, 2010; Zhu et al, 2010), which plays a pivotal role in the tumor progression; secondly, altered expression of PDCD10 is observed in some tumors (Barrier et al, 2005; Fu et al, 2016; Lambertz et al, 2015; Yang et al, 2017); thirdly, the co-incidence of CCM and brain tumors is reported: CCM with low-grade astrocytoma(Zhang et al, 2012) or with GBM (Mian et al, 2012; Wilson et al, 2014) have been shown and a direct association of PDCD10/CCM3 mutation with multiple meningioma has also been reported (Fauth et al, 2015; Labauge et al, 2009; Riant et al, 2013). All these data strongly suggest that PDCD10 should play a role in tumor development. However, few publications deal with the function of tumor-originated PDCD10 and do not reach consistent results until now. For example, Barrier *et al* (Barrier et al, 2005) demonstrated that over-expression of PDCD10 was associated with poor prognosis of colorectal cancer patients. Fu et al (Fu et al, 2016) also showed that down-regulation of PDCD10, a direct target of miR-103, could suppress prostate cancer proliferation and migration. Another study indicated that the down-regulation of

PDCD10 modulated by miRNA-425-5p was involved in chemo-resistance in colorectal cancer cells (Zhang et al, 2016). Nevertheless, little is known about its role in GBM until now. More recently, the role of PDCD10 in GBM has been attracted much attention. Our group has previously demonstrated that PDCD10 was often absent in ECs of tumor vessels as well as in GBM cells of human GBM; PDCD10 expression was associated with a higher microvessel density in GBM (Lambertz et al, 2015). Further study of the interaction between ECs and GBM cells indicated that PDCD10-ablation in ECs activated proliferation-, adhesion-, invasion- and migration of GBM cells *in vitro* (Zhu et al, 2016). These data strongly indicated a potential function of PDCD10 in GBM progression, which raised our interest to further explore the role of PDCD10 in GBM and the potential mechanism. The present study demonstrated that knockdown of PDCD10 in GBM cells resulted in the activation of GBM cells via significant upregulation of EphB4 mRNA and protein expression and consequently a remarkable increase in the EphB4 kinase activity, which was completely reversed by the treatment with a specific EphB4 kinase inhibitor NVP. These results indicate that EphB4 acts downstream of PDCD10 in GBM cells. The functional study demonstrated that upon NVP treatment, the inhibition of EphB4 kinase activity can inhibit the aggressive behavior in shPDCD10 GBM cells (shPDCD10 TCs), as well as hinder rapid tumor formation and proliferation, thereby leading to a reduction of the tumor mass in PDCD10 knockdown tumor. These findings provide evidence that the tumor-promoting effect resulted from PDCD10 knockdown is mediated by the upregulation/activation of EphB4. Both forward and reverse signaling by the EphB4/ephrinB2 interaction is context-dependent and can vary from one cancer type to another (Lodola et al, 2017). EphB4 is upregulated in GBM and the EphB4/ephrinB2 pathway is involved in the neo-angiogenesis (Groppa et al, 2018), tumors progression, the prognosis of GBM (Chen et al, 2013; Tu et al, 2012; Uhl et al, 2018), and in the resistance to anti-angiogenesis therapy (Uhl et al, 2018). These data underscore the oncogenic function of EphB4 in GBM and suggest EphB4 as a promising therapeutic target (Day et al, 2014). Pharmacologically targeting EphB4 has emerged as a strategy

against numerous cancers (Salgia et al, 2018). Soluble EphB4 (sEphB4) is a soluble decoy of EphB4 that blocks EphB4-Ephrin-B2 bi-directional signaling. The anti-tumor activities of sEphB4 have been shown in multiple tumor models (Djokovic et al, 2010; Scehnet et al, 2009). Another interesting option to inhibit EphB4 is the use of humanized monoclonal anti-EphB4. Krasnoperov et al. (Krasnoperov et al, 2010) described two EphB4 antibodies MAb131 and MAb47 that inhibit angiogenesis and tumor growth in a non–small-cell lung cancer cell line with distinct mechanisms. Of particular note, the application of small molecule compounds that specifically act as a kinase inhibitor is more feasible to interfere with the activity of kinases such as EphB4. NVP is a small molecule that selectively inhibits the tyrosine kinase activity of EphB4 (Martiny-Baron et al, 2010). Becerikli et al. (Becerikli et al, 2015) showed that NVP inhibited EphB4 autophosphorylation, the reduced cell growth rate of synovial sarcoma and fibrosarcoma cells *in vitro* and hampered sarcoma lung metastasis *in vivo*. Inhibition of EphB4 by NVP could overcome the acquired resistance to cisplatin in melanoma xenograft models (Yang et al, 2015). By using NVP, we previously identified the EphB4-Erk1/2 as downstream signaling of the Dll4-Notch pathway in endothelial cells. This is an important mechanism for the pro-angiogenic and anti-apoptotic function resulting from the knockdown of endothelial PDCD10 (You et al, 2017). The present study adds new evidence that NVP is able to reverse shPDCD10-induced activation of EphB4 thus its tumor-promoting effect via inhibiting EphB4 in GBM cells and a mouse model of human GBM. Moreover, we demonstrated that the conditioned medium from stable knockdown of PDCD10 in GBM cells significantly promoted migration and adhesion of HUVECs *in vitro*. Meantime, we also noted CD31-positive cells and vessel-like structures exclusively on the sections from PDCD10-knockdown xenograft tumors. Some of these microvessels contained blood cells suggesting the formation of functional vessels after knockdown of PDCD10 in tumors. Further study demonstrated that 8 of 55 tested factors were were increased by more than 2-fold after the loss of tumor-originated of PDCD10 in GBM cells, and these eight soluble factors played crucial roles in regulating tumor cell proliferation,

migration and invasion as well as angiogenesis (Hoelzinger et al, 2007). For example, angiogenin, which plays an essential role in endothelial cell proliferation and is necessary for angiogenesis (Kishimoto et al, 2005), is the most significantly increased soluble factor and has a prominent role in the pathology of cancer due to its functions in angiogenesis and cell survival (Sheng et al, 2016). The upregulation of angiogenin is also reported to be associated with poor prognosis in some human cancers and is strongly correlated with an invasive cancer phenotype involving the stimulation of matrix metallopeptidase-2 (MMP2) expression through activation of Erk1/2 (Miyake et al, 2015). The second highest upregulated factor HGF is secreted from both GBM cells and stromal cells (Abounader et al, 2005; Koochekpour et al, 1997), followed by activation of the HGF/Met pathway and promotion of the cells proliferation, migration and invasion via autocrine loop (Abounader et al, 2005; Cruickshanks et al, 2017) thereby contributing to oncogenesis and tumor progression in several cancers and promoting aggressive cellular invasiveness that is strongly linked to tumor metastasis (Cecchi et al, 2012). Moreover, HGF is the most potent chemotactic factor and associated with cell motility (Brockmann et al, 2003). Endoglin, another upregulated factor, is a homodimeric cell membrane glycoprotein receptor for transforming growth factor β and bone morphogenetic proteins. Its expression is implicated in the development of resistance to vascular endothelial growth factor (VEGF)-targeted tumor therapy (Rosen et al, 2014). Thus, we believe that all these upregulated soluble factors resulting from PDCD10 knockdown could synergistically act on ECs to trigger ECs adhesion and migration, and eventually stimulate tumor growth and tumor invasion.

The secreted factors from shPDCD10 TCs, components of the tumor environment formed by the interaction between the tumor cells and non-tumor cells through direct cell-cell contact and/or the secreted factors from the cells, plays an essential role for tumorigenesis, metastasis and progression (Hoelzinger et al, 2007; Owusu et al, 2017; Wang et al, 2017). The tumor environment does not only play a key role in providing nutrients and maintaining the stem cells of tumors, but also involves in the immunity response and

therapy resistance (Owusu et al, 2017; Persano et al, 2013; Wang et al, 2017). That's why the prognosis of GBM patients do not improve even though some new therapies or drugs targeting one of the growth factors or their receptors have been developed during decades since targeting a single factor or receptor has shown limited benefits for GBM patients in this microenvironment (Thomas et al, 2014). For example, anti-VEGF treatment can reduce the blood supply of the tumor, but increases tumor cell invasion in glioblastoma via increased HIFα expression due to hypoxia (Keunen et al, 2011). Anit-RAF treatment increased the secretion of HGF from stromal cells, mediating drug resistance (Straussman et al, 2012). Therefore, targeting a single pathway or molecules is limited to improve the prognosis and the strategy targeting GBM cells at multiple levels should be applied and more effective against tumor progression. As demonstrated in this study, PDCD10 knockdown in GBM cells does not only activate the GBM cells themselves via upregulation/activation EphB4 but also could stimulate the release of multiple angiogenic-related factors, thereby altering the microenvironment, simultaneously activating survival signaling pathways of GBM cells and ECs, promoting tumor growth and angiogenesis. These findings also provide the evidence that PDCD10 might be a potential target for GBM therapy in the future.

In conclusion, knockdown of PDCD10 activated TCs and promoted tumor growth via significant upregulation of EphB4 expression. Knockdown of tumoral PDCD10 can trigger HUVECs through the increase in release of proangiogenic factors. Therefore, targeting PDCD10 together with its downstream effector EphB4 might be an effective strategy for personalized therapy in GBM patients with PDCD10-deficiency.

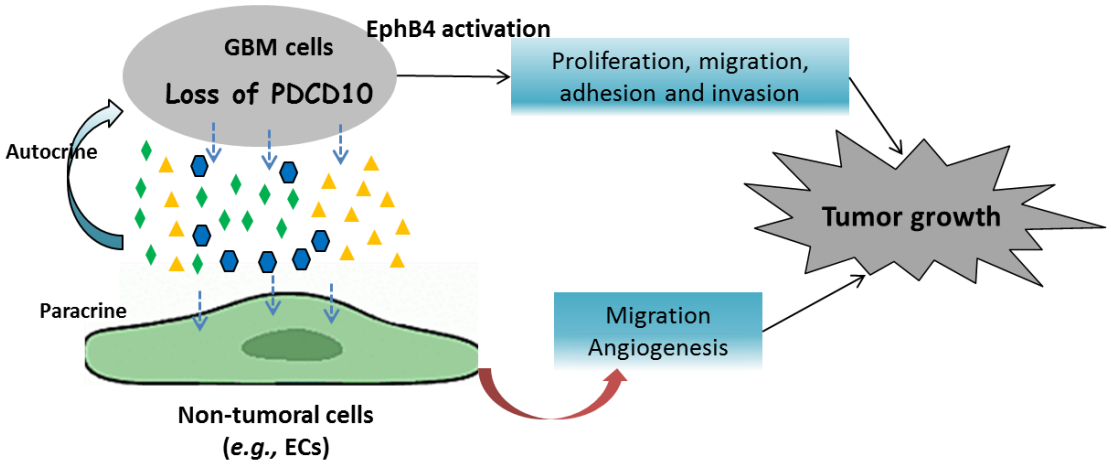

Figure 15 Schematic summary for the effect of PDCD10 knockdown on GBM cells and ECs

Loss of PDCD10 in GBM cells could promote GBM cells proliferation, adhesion, migration and invasion through upregulation/activation of EphB4. Additionally, shPDCD10 TCs resulted in increasing release of proangiogenic factors and activation of GBM and non-tumoral cells (e.g. ECs). All these effects synergistically promoted tumor growth. These data suggested that PDCD10 displayed a tumor-suppressor like function.

5. Summary

Programmed cell death 10 (PDCD10) plays crucial roles in multiple cellular processes. Our laboratory has previously demonstrated that loss of endothelial PDCD10 stimulated endothelial angiogenesis and activated glioblastoma (GBM) cells and promoted GBM tumor growth. The aims of present study are to further explore that the role of tumoral PDCD10 in tumor cells (TCs) and to check whether EphB4 is involved in these effects; and to test the possible influence of tumoral PDCD10 on endothelial cells (ECs). To this end, the phenotype of TCs lines and the EphB4 expression/activity were investigated in PDCD10 knockdown (shPDCD10) TCs. The endothelia angiogenesis was studied in HUVECs after treatment with the conditioned media (CM) from shPDCD10-TCs. In present study, we demonstrated that knockdown of PDCD10 in TCs resulted in the activation of shPDCD10-TCs via significant upregulation of EphB4 expression and a remarkable increase in the EphB4 kinase activity. Treatment of shPDCD10-TCs with NVP inhibited the activation of EphB4 kinase, suppressed the aggressive behavior of shPDCD10 TCs *in vitro*, and hindered tumor growth in PDCD10 knockdown tumor. These findings indicated that the upregulation/activation of EphB4 is involved in the tumor-promoting effect resulted from PDCD10 knockdown. In addition, treatment of HUVECs with CM from shPDCD10-TCs promoted the angiogenesis *in vitro.* The protein array revealed that the level of 8 of 55 angiogenic factors was significantly upregulated in the CM from the shPDCD10-TCs, which may play crucial roles in stimulation of endothelial angiogenesis. In conclusion, knockdown of PDCD10 activated TCs and promoted tumor growth via significant upregulation of EphB4 expression. Knockdown of tumoral PDCD10 can trigger HUVECs through the increase in release of proangiogenic factors. Therefore, targeting PDCD10 together with its downstream effector EphB4 might be an effective strategy for personalized therapy in GBM patients with PDCD10-deficiency.

Zusammenfassung

Das Protein „programmierte Zelltod 10“ (PDCD10) spielt eine entscheidende Rolle in mehreren zellulären Prozessen. Studien zeigten bereits, dass der Verlust von endothelialem PDCD10 die endotheliale Angiogenese und die Aktivierung von Glioblastom (GBM)-Zellen stimuliert und das Tumorwachstum des GBM fördert. Das Ziel dieser Studie ist es die Rolle von PDCD10 in Tumorzellen (TCs) und Endothelzellen (ECs) weiter zu erforschen und eine mögliche Beteiligung des Ephrin Rezeptors EphB4, an diesen Signalwegen nachzuweisen. Zu diesem Zweck wurde der Phänotyp von TCs-Linien und die EphB4-Expression/Aktivität in PDCD10-Knockdown (shPDCD10) TCs untersucht, so wie die Endothel-Angiogenese in der Endothelzelllinie HUVEC. Die Ergebnisse deuten darauf hin, dass die Hochregulierung/Aktivierung von EphB4 an dem tumorfördernden Effekt, entstanden aus einem PDCD10 Knockdown, beteiligt ist. Dies konnte durch die Behandlung von shPDCD10-TCs mit dem EphB4-Kinase-Inhibitor NVP-BHG712 *in vitro* und *in vivo* bestätigt werden. Um den Einfluss von PDCD10 auf die Angiogenese weiter zu untersuchen wurden HUVECs mit konditioniertem Medium der shPDCD10-TCs behandelt und ein Proteinarray für die Identifikation möglicher Angiogenese Faktoren durchgeführt. Hier wurden 8 Faktoren identifiziert, die signifikant hochreguliert waren und eine Rolle bei der Stimulation der endothelialen Angiogenese spielen könnten. Zusammenfassend konnte gezeigt werden, dass der Knockdown von PDCD10 in TCs das Tumorwachstum über die Hochregulierung der EphB4-Expression und einen Anstieg der EphB4-Kinase-Aktivität *in vitro* und *in vivo* fördert. Des Weiteren konnte nachgewiesen werden das der Knockdown des tumoralen PDCD10 in HUVECs durch die erhöhte Freisetzung von proangiogenen Faktoren das Tumorwachstum fördern. Auf lange Sicht könnte das Targeting von PDCD10 zusammen mit seinem Downstream-Effektor EphB4 eine effektive Strategie für die personalisierte Therapie bei GBM-Patienten mit PDCD10-Mangel sein.

6. Reference

1 Abounader R., Laterra J. (2005): Scatter factor/hepatocyte growth factor in brain tumor growth and angiogenesis. Neuro Oncol. 7, 436-451.

2 Alexander B. M., Cloughesy T. F. (2017): Adult Glioblastoma. J Clin Oncol. 35, 2402-2409.

3 Alifieris C., Trafalis D. T. (2015): Glioblastoma multiforme: Pathogenesis and treatment. Pharmacol Ther. 152, 63-82.

4 Barrier A., Lemoine A., Boelle P. Y., Tse C., Brault D., Chiappini F., Breittschneider J., Lacaine F., Houry S., Huguier M., Van der Laan M. J., Speed T., Debuire B., Flahault A., Dudoit S. (2005): Colon cancer prognosis prediction by gene expression profiling. Oncogene. 24, 6155-6164.

5 Becerikli M., Merwart B., Lam M. C., Suppelna P., Rittig A., Mirmohammedsadegh A., Stricker I., Theiss C., Singer B. B., Jacobsen F., Steinstraesser L. (2015): EPHB4 tyrosine-kinase receptor expression and biological significance in soft tissue sarcoma. Int J Cancer. 136, 1781-1791.

6 Bergametti F., Denier C., Labauge P., Arnoult M., Boetto S., Clanet M., Coubes P., Echenne B., Ibrahim R., Irthum B., Jacquet G., Lonjon M., Moreau J. J., Neau J. P., Parker F., Tremoulet M., Tournier-Lasserve E., Societe Francaise de N. (2005): Mutations within the programmed cell death 10 gene cause cerebral cavernous malformations. Am J Hum Genet. 76, 42-51.

7 Borikova A. L., Dibble C. F., Sciaky N., Welch C. M., Abell A. N., Bencharit S., Johnson G. L. (2010): Rho kinase inhibition rescues the endothelial cell cerebral cavernous malformation phenotype. J Biol Chem. 285, 11760-11764.

8 Brantley-Sieders D. M., Jiang A., Sarma K., Badu-Nkansah A., Walter D. L., Shyr Y., Chen J. (2011): Eph/ephrin profiling in human breast cancer reveals significant associations between expression level and clinical outcome. PLoS One. 6, e24426.

9 Brockmann M. A., Ulbricht U., Gruner K., Fillbrandt R., Westphal M., Lamszus K. (2003): Glioblastoma and cerebral microvascular endothelial cell migration in response

to tumor-associated growth factors. Neurosurgery. 52, 1391-1399; discussion 1399.

10 Cecchi F., Rabe D. C., Bottaro D. P. (2012): Targeting the HGF/Met signaling pathway in cancer therapy. Expert Opin Ther Targets. 16, 553-572.

11 Chen L., Tanriover G., Yano H., Friedlander R., Louvi A., Gunel M. (2009): Apoptotic functions of PDCD10/CCM3, the gene mutated in cerebral cavernous malformation 3. Stroke. 40, 1474-1481.

12 Chen T., Liu X., Yi S., Zhang J., Ge J., Liu Z. (2013): EphB4 is overexpressed in gliomas and promotes the growth of glioma cells. Tumour Biol. 34, 379-385.

13 Cheng N., Brantley D. M., Chen J. (2002): The ephrins and Eph receptors in angiogenesis. Cytokine Growth Factor Rev. 13, 75-85.

14 Cloughesy T. F., Cavenee W. K., Mischel P. S. (2014): Glioblastoma: from molecular pathology to targeted treatment. Annu Rev Pathol. 9, 1-25.

15 Cruickshanks N., Zhang Y., Yuan F., Pahuski M., Gibert M., Abounader R. (2017): Role and Therapeutic Targeting of the HGF/MET Pathway in Glioblastoma. Cancers (Basel). 9

16 Day B. W., Stringer B. W., Boyd A. W. (2014): Eph receptors as therapeutic targets in glioblastoma. Br J Cancer. 111, 1255-1261.

17 Djokovic D., Trindade A., Gigante J., Badenes M., Silva L., Liu R., Li X., Gong M., Krasnoperov V., Gill P. S., Duarte A. (2010): Combination of Dll4/Notch and Ephrin-B2/EphB4 targeted therapy is highly effective in disrupting tumor angiogenesis. BMC Cancer. 10, 641.

18 Draheim K. M., Fisher O. S., Boggon T. J., Calderwood D. A. (2014): Cerebral cavernous malformation proteins at a glance. J Cell Sci. 127, 701-707.

19 Fauth C., Rostasy K., Rath M., Gizewski E., Lederer A. G., Sure U., Zschocke J., Felbor U. (2015): Highly variable intrafamilial manifestations of a CCM3 mutation ranging from acute childhood cerebral haemorrhage to late-onset meningiomas. Clin Neurol Neurosurg. 128, 41-43.

20 Ferguson B. D., Liu R., Rolle C. E., Tan Y. H., Krasnoperov V., Kanteti R.,

Tretiakova M. S., Cervantes G. M., Hasina R., Hseu R. D., Iafrate A. J., Karrison T., Ferguson M. K., Husain A. N., Faoro L., Vokes E. E., Gill P. S., Salgia R. (2013): The EphB4 receptor tyrosine kinase promotes lung cancer growth: a potential novel therapeutic target. PLoS One. 8, e67668.

21 Fidalgo M., Fraile M., Pires A., Force T., Pombo C., Zalvide J. (2010): CCM3/PDCD10 stabilizes GCKIII proteins to promote Golgi assembly and cell orientation. J Cell Sci. 123, 1274-1284.

22 Fischer A., Zalvide J., Faurobert E., Albiges-Rizo C., Tournier-Lasserve E. (2013): Cerebral cavernous malformations: from CCM genes to endothelial cell homeostasis. Trends Mol Med. 19, 302-308.

23 Fu X., Zhang W., Su Y., Lu L., Wang D., Wang H. (2016): MicroRNA-103 suppresses tumor cell proliferation by targeting PDCD10 in prostate cancer. Prostate. 76, 543-551.

24 Groppa E., Brkic S., Uccelli A., Wirth G., Korpisalo-Pirinen P., Filippova M., Dasen B., Sacchi V., Muraro M. G., Trani M., Reginato S., Gianni-Barrera R., Yla-Herttuala S., Banfi A. (2018): EphrinB2/EphB4 signaling regulates non-sprouting angiogenesis by VEGF. EMBO Rep. 19

25 Hasina R., Mollberg N., Kawada I., Mutreja K., Kanade G., Yala S., Surati M., Liu R., Li X., Zhou Y., Ferguson B. D., Nallasura V., Cohen K. S., Hyjek E., Mueller J., Kanteti R., El Hashani E., Kane D., Shimada Y., Lingen M. W., Husain A. N., Posner M. C., Waxman I., Villaflor V. M., Ferguson M. K., Varticovski L., Vokes E. E., Gill P., Salgia R. (2013): Critical role for the receptor tyrosine kinase EPHB4 in esophageal cancers. Cancer Res. 73, 184-194.

26 He Y., Zhang H., Yu L., Gunel M., Boggon T. J., Chen H., Min W. (2010): Stabilization of VEGFR2 signaling by cerebral cavernous malformation 3 is critical for vascular development. Sci Signal. 3, ra26.

27 Hegi M. E., Diserens A. C., Gorlia T., Hamou M. F., de Tribolet N., Weller M., Kros J. M., Hainfellner J. A., Mason W., Mariani L., Bromberg J. E., Hau P., Mirimanoff R. O.,

Cairncross J. G., Janzer R. C., Stupp R. (2005): MGMT gene silencing and benefit from temozolomide in glioblastoma. N Engl J Med. 352, 997-1003.

28 Heroult M., Schaffner F., Augustin H. G. (2006): Eph receptor and ephrin ligand-mediated interactions during angiogenesis and tumor progression. Exp Cell Res. 312, 642-650.

29 Hoelzinger D. B., Demuth T., Berens M. E. (2007): Autocrine factors that sustain glioma invasion and paracrine biology in the brain microenvironment. J Natl Cancer Inst. 99, 1583-1593.

30 Jenny Zhou H., Qin L., Zhang H., Tang W., Ji W., He Y., Liang X., Wang Z., Yuan Q., Vortmeyer A., Toomre D., Fuh G., Yan M., Kluger M. S., Wu D., Min W. (2016): Endothelial exocytosis of angiopoietin-2 resulting from CCM3 deficiency contributes to cerebral cavernous malformation. Nat Med. 22, 1033-1042.

31 Keunen O., Johansson M., Oudin A., Sanzey M., Rahim S. A., Fack F., Thorsen F., Taxt T., Bartos M., Jirik R., Miletic H., Wang J., Stieber D., Stuhr L., Moen I., Rygh C. B., Bjerkvig R., Niclou S. P. (2011): Anti-VEGF treatment reduces blood supply and increases tumor cell invasion in glioblastoma. Proc Natl Acad Sci U S A. 108, 3749-3754.

32 Kishimoto K., Liu S., Tsuji T., Olson K. A., Hu G. F. (2005): Endogenous angiogenin in endothelial cells is a general requirement for cell proliferation and angiogenesis. Oncogene. 24, 445-456.

33 Klein R. (2004): Eph/ephrin signaling in morphogenesis, neural development and plasticity. Curr Opin Cell Biol. 16, 580-589.

34 Koochekpour S., Jeffers M., Rulong S., Taylor G., Klineberg E., Hudson E. A., Resau J. H., Vande Woude G. F. (1997): Met and hepatocyte growth factor/scatter factor expression in human gliomas. Cancer Res. 57, 5391-5398.

35 Krasnoperov V., Kumar S. R., Ley E., Li X., Scehnet J., Liu R., Zozulya S., Gill P. S. (2010): Novel EphB4 monoclonal antibodies modulate angiogenesis and inhibit tumor growth. Am J Pathol. 176, 2029-2038.

36 Kumar S. R., Scehnet J. S., Ley E. J., Singh J., Krasnoperov V., Liu R., Manchanda

P. K., Ladner R. D., Hawes D., Weaver F. A., Beart R. W., Singh G., Nguyen C., Kahn M., Gill P. S. (2009): Preferential induction of EphB4 over EphB2 and its implication in colorectal cancer progression. Cancer Res. 69, 3736-3745.

37 Labauge P., Fontaine B., Neau J. P., Bergametti F., Riant F., Blecon A., Marchelli F., Arnoult M., Lannuzel A., Clanet M., Olschwang S., Denier C., Tournier-Lasserve E. (2009): Multiple dural lesions mimicking meningiomas in patients with CCM3/PDCD10 mutations. Neurology. 72, 2044-2046.

38 Lambertz N., El Hindy N., Kreitschmann-Andermahr I., Stein K. P., Dammann P., Oezkan N., Mueller O., Sure U., Zhu Y. (2015): Downregulation of programmed cell death 10 is associated with tumor cell proliferation, hyperangiogenesis and peritumoral edema in human glioblastoma. BMC Cancer. 15, 759.

39 Lin C., Meng S., Zhu T., Wang X. (2010): PDCD10/CCM3 acts downstream of {gamma}-protocadherins to regulate neuronal survival. J Biol Chem. 285, 41675-41685.

40 Liu R., Ferguson B. D., Zhou Y., Naga K., Salgia R., Gill P. S., Krasnoperov V. (2013): EphB4 as a therapeutic target in mesothelioma. BMC Cancer. 13, 269.

41 Lodola A., Giorgio C., Incerti M., Zanotti I., Tognolini M. (2017): Targeting Eph/ephrin system in cancer therapy. Eur J Med Chem. 142, 152-162.

42 Louvi A., Chen L., Two A. M., Zhang H., Min W., Gunel M. (2011): Loss of cerebral cavernous malformation 3 (Ccm3) in neuroglia leads to CCM and vascular pathology. Proc Natl Acad Sci U S A. 108, 3737-3742.

43 Ma X., Zhao H., Shan J., Long F., Chen Y., Chen Y., Zhang Y., Han X., Ma D. (2007): PDCD10 interacts with Ste20-related kinase MST4 to promote cell growth and transformation via modulation of the ERK pathway. Mol Biol Cell. 18, 1965-1978.

44 Madsen C. D., Hooper S., Tozluoglu M., Bruckbauer A., Fletcher G., Erler J. T., Bates P. A., Thompson B., Sahai E. (2015): STRIPAK components determine mode of cancer cell migration and metastasis. Nat Cell Biol. 17, 68-80.

45 Marchi S., Corricelli M., Trapani E., Bravi L., Pittaro A., Delle Monache S., Ferroni L., Patergnani S., Missiroli S., Goitre L., Trabalzini L., Rimessi A., Giorgi C., Zavan B.,

Cassoni P., Dejana E., Retta S. F., Pinton P. (2015): Defective autophagy is a key feature of cerebral cavernous malformations. EMBO Mol Med. 7, 1403-1417.

46 Marquet G., Dameron O., Saikali S., Mosser J., Burgun A. (2007): Grading glioma tumors using OWL-DL and NCI Thesaurus. AMIA Annu Symp Proc. 508-512.

47 Martiny-Baron G., Holzer P., Billy E., Schnell C., Brueggen J., Ferretti M., Schmiedeberg N., Wood J. M., Furet P., Imbach P. (2010): The small molecule specific EphB4 kinase inhibitor NVP-BHG712 inhibits VEGF driven angiogenesis. Angiogenesis. 13, 259-267.

48 Mellitzer G., Xu Q., Wilkinson D. G. (1999): Eph receptors and ephrins restrict cell intermingling and communication. Nature. 400, 77-81.

49 Mian M. K., Nahed B. V., Walcott B. P., Ogilvy C. S., Curry W. T. (2012): Glioblastoma multiforme and cerebral cavernous malformations: intersection of pathophysiologic pathways. J Clin Neurosci. 19, 884-886.

50 Miyake M., Goodison S., Lawton A., Gomes-Giacoia E., Rosser C. J. (2015): Angiogenin promotes tumoral growth and angiogenesis by regulating matrix metallopeptidase-2 expression via the ERK1/2 pathway. Oncogene. 34, 890-901.

51 Murai K. K., Pasquale E. B. (2003): 'Eph'ective signaling: forward, reverse and crosstalk. J Cell Sci. 116, 2823-2832.

52 Nickel A. C., Wan X. Y., Saban D. V., Weng Y. L., Zhang S., Keyvani K., Sure U., Zhu Y. (2019): Loss of programmed cell death 10 activates tumor cells and leads to temozolomide-resistance in glioblastoma. J Neurooncol. 141, 31-41.

53 Owusu B. Y., Galemmo R., Janetka J., Klampfer L. (2017): Hepatocyte Growth Factor, a Key Tumor-Promoting Factor in the Tumor Microenvironment. Cancers (Basel). 9

54 Persano L., Rampazzo E., Basso G., Viola G. (2013): Glioblastoma cancer stem cells: role of the microenvironment and therapeutic targeting. Biochem Pharmacol. 85, 612-622.

55 Petit N., Blecon A., Denier C., Tournier-Lasserve E. (2006): Patterns of expression of the three cerebral cavernous malformation (CCM) genes during embryonic and

postnatal brain development. Gene Expr Patterns. 6, 495-503.

56 Riant F., Bergametti F., Fournier H. D., Chapon F., Michalak-Provost S., Cecillon M., Lejeune P., Hosseini H., Choe C., Orth M., Bernreuther C., Boulday G., Denier C., Labauge P., Tournier-Lasserve E. (2013): CCM3 Mutations Are Associated with Early-Onset Cerebral Hemorrhage and Multiple Meningiomas. Mol Syndromol. 4, 165-172.

57 Rosen L. S., Gordon M. S., Robert F., Matei D. E. (2014): Endoglin for targeted cancer treatment. Curr Oncol Rep. 16, 365.

58 Salgia R., Kulkarni P., Gill P. S. (2018): EphB4: A promising target for upper aerodigestive malignancies. Biochim Biophys Acta Rev Cancer. 1869, 128-137.

59 Scehnet J. S., Ley E. J., Krasnoperov V., Liu R., Manchanda P. K., Sjoberg E., Kostecke A. P., Gupta S., Kumar S. R., Gill P. S. (2009): The role of Ephs, Ephrins, and growth factors in Kaposi sarcoma and implications of EphrinB2 blockade. Blood. 113, 254-263.

60 Schleider E., Stahl S., Wustehube J., Walter U., Fischer A., Felbor U. (2011): Evidence for anti-angiogenic and pro-survival functions of the cerebral cavernous malformation protein 3. Neurogenetics. 12, 83-86.

61 Sheng J., Xu Z. (2016): Three decades of research on angiogenin: a review and perspective. Acta Biochim Biophys Sin (Shanghai). 48, 399-410.

62 Shenkar R., Shi C., Rebeiz T., Stockton R. A., McDonald D. A., Mikati A. G., Zhang L., Austin C., Akers A. L., Gallione C. J., Rorrer A., Gunel M., Min W., De Souza J. M., Lee C., Marchuk D. A., Awad I. A. (2015): Exceptional aggressiveness of cerebral cavernous malformation disease associated with PDCD10 mutations. Genet Med. 17, 188-196.

63 Straussman R., Morikawa T., Shee K., Barzily-Rokni M., Qian Z. R., Du J., Davis A., Mongare M. M., Gould J., Frederick D. T., Cooper Z. A., Chapman P. B., Solit D. B., Ribas A., Lo R. S., Flaherty K. T., Ogino S., Wargo J. A., Golub T. R. (2012): Tumour micro-environment elicits innate resistance to RAF inhibitors through HGF secretion. Nature. 487, 500-504.

64 Thomas A. A., Brennan C. W., DeAngelis L. M., Omuro A. M. (2014): Emerging therapies for glioblastoma. JAMA Neurol. 71, 1437-1444.

65 Tu Y., He S., Fu J., Li G., Xu R., Lu H., Deng J. (2012): Expression of EphrinB2 and EphB4 in glioma tissues correlated to the progression of glioma and the prognosis of glioblastoma patients. Clin Transl Oncol. 14, 214-220.

66 Turkalp Z., Karamchandani J., Das S. (2014): IDH mutation in glioma: new insights and promises for the future. JAMA Neurol. 71, 1319-1325.

67 Uhl C., Markel M., Broggini T., Nieminen M., Kremenetskaia I., Vajkoczy P., Czabanka M. (2018): EphB4 mediates resistance to antiangiogenic therapy in experimental glioma. Angiogenesis. 21, 873-881.

68 Urbanska K., Sokolowska J., Szmidt M., Sysa P. (2014): Glioblastoma multiforme - an overview. Contemp Oncol (Pozn). 18, 307-312.

69 Urfali-Mamatoglu C., Kazan H. H., Gunduz U. (2018): Dual function of programmed cell death 10 (PDCD10) in drug resistance. Biomed Pharmacother. 101, 129-136.

70 Verhaak R. G., Hoadley K. A., Purdom E., Wang V., Qi Y., Wilkerson M. D., Miller C. R., Ding L., Golub T., Mesirov J. P., Alexe G., Lawrence M., O'Kelly M., Tamayo P., Weir B. A., Gabriel S., Winckler W., Gupta S., Jakkula L., Feiler H. S., Hodgson J. G., James C. D., Sarkaria J. N., Brennan C., Kahn A., Spellman P. T., Wilson R. K., Speed T. P., Gray J. W., Meyerson M., Getz G., Perou C. M., Hayes D. N., Cancer Genome Atlas Research N. (2010): Integrated genomic analysis identifies clinically relevant subtypes of glioblastoma characterized by abnormalities in PDGFRA, IDH1, EGFR, and NF1. Cancer Cell. 17, 98-110.

71 Vollmann-Zwerenz A., Leidgens V., Feliciello G., Klein C. A., Hau P. (2020): Tumor Cell Invasion in Glioblastoma. Int J Mol Sci. 21

72 Wang Q., Hu B., Hu X., Kim H., Squatrito M., Scarpace L., deCarvalho A. C., Lyu S., Li P., Li Y., Barthel F., Cho H. J., Lin Y. H., Satani N., Martinez-Ledesma E., Zheng S., Chang E., Sauve C. G., Olar A., Lan Z. D., Finocchiaro G., Phillips J. J., Berger M. S.,

Gabrusiewicz K. R., Wang G., Eskilsson E., Hu J., Mikkelsen T., DePinho R. A., Muller F., Heimberger A. B., Sulman E. P., Nam D. H., Verhaak R. G. W. (2017): Tumor Evolution of Glioma-Intrinsic Gene Expression Subtypes Associates with Immunological Changes in the Microenvironment. Cancer Cell. 32, 42-56 e46.

73 Wang Y., Liu H., Zhang Y., Ma D. (1999): cDNA cloning and expression of an apoptosis-related gene, humanTFAR15 gene. Sci China C Life Sci. 42, 323-329.

74 Wilson D. M., Cohen B., Keshari K., Vogel H., Steinberg G., Dillon W. (2014): Case report: glioblastoma multiforme complicating familial cavernous malformations. Clin Neuroradiol. 24, 293-296.

75 Xia G., Kumar S. R., Stein J. P., Singh J., Krasnoperov V., Zhu S., Hassanieh L., Smith D. L., Buscarini M., Broek D., Quinn D. I., Weaver F. A., Gill P. S. (2006): EphB4 receptor tyrosine kinase is expressed in bladder cancer and provides signals for cell survival. Oncogene. 25, 769-780.

76 Yang D., Wang J. J., Li J. S., Xu Q. Y. (2017): MiR-103 Functions as a Tumor Suppressor by Directly Targeting Programmed Cell Death 10 in NSCLC. Oncol Res.

77 Yang X., Yang Y., Tang S., Tang H., Yang G., Xu Q., Wu J. (2015): EphB4 inhibitor overcome the acquired resistance to cisplatin in melanomas xenograft model. J Pharmacol Sci. 129, 65-71.

78 You C., Sandalcioglu I. E., Dammann P., Felbor U., Sure U., Zhu Y. (2013): Loss of CCM3 impairs DLL4-Notch signalling: implication in endothelial angiogenesis and in inherited cerebral cavernous malformations. J Cell Mol Med. 17, 407-418.

79 You C., Zhao K., Dammann P., Keyvani K., Kreitschmann-Andermahr I., Sure U., Zhu Y. (2017): EphB4 forward signalling mediates angiogenesis caused by CCM3/PDCD10-ablation. J Cell Mol Med. 21, 1848-1858.

80 Zhang J. Y., Ming Z. Y., Wu A. H. (2012): Is cerebral cavernous malformation a pre-glioma lesion? Chin Med J (Engl). 125, 4511-4513.

81 Zhang Y., Hu X., Miao X., Zhu K., Cui S., Meng Q., Sun J., Wang T. (2016): MicroRNA-425-5p regulates chemoresistance in colorectal cancer cells via regulation of

Programmed Cell Death 10. J Cell Mol Med. 20, 360-369.

82 Zheng X., Xu C., Di Lorenzo A., Kleaveland B., Zou Z., Seiler C., Chen M., Cheng L., Xiao J., He J., Pack M. A., Sessa W. C., Kahn M. L. (2010): CCM3 signaling through sterile 20-like kinases plays an essential role during zebrafish cardiovascular development and cerebral cavernous malformations. J Clin Invest. 120, 2795-2804.

83 Zhou Z., Tang A. T., Wong W. Y., Bamezai S., Goddard L. M., Shenkar R., Zhou S., Yang J., Wright A. C., Foley M., Arthur J. S., Whitehead K. J., Awad I. A., Li D. Y., Zheng X., Kahn M. L. (2016): Cerebral cavernous malformations arise from endothelial gain of MEKK3-KLF2/4 signalling. Nature. 532, 122-126.

84 Zhu Y., Wu Q., Xu J. F., Miller D., Sandalcioglu I. E., Zhang J. M., Sure U. (2010): Differential angiogenesis function of CCM2 and CCM3 in cerebral cavernous malformations. Neurosurg Focus. 29, E1.

85 Zhu Y., Zhao K., Prinz A., Keyvani K., Lambertz N., Kreitschmann-Andermahr I., Lei T., Sure U. (2016): Loss of endothelial programmed cell death 10 activates glioblastoma cells and promotes tumor growth. Neuro Oncol. 18, 538-548.

7.1 Abbreviation

AKT Protein kinase B

APS Ammonium persulfate

ATRX ATP-dependent helicase ATRX, X-linked helicase II

bFGF Basic fibroblast growth factor

CCM Cerebral cavernous malformations

CCM3 Cerebral cavernous malformation 3

CCMEC CCM patient endothelial cells

CDKN2A cyclin-dependent kinase Inhibitor 2A

CM Conditioned medium

CNS Central nervous system

Dll4 Delta like ligand 4

DMEM Dulbecco's Modified Eagle Medium

DMSO Dimethyl sulfoxide

DTT -Dithiothreitol

EC/ECs Endothelial cell/Endothelial cells

ECGM Endothelial cell growth medium

EGF Epidermal growth factor

EGFR Epidermal growth factor receptor

Erk1/2 Extracellular signal regulated kinase 1/2

EphB4 erythropoietin-producing human hepatocellular carcinoma B4

EV Empty vector

FBS Fetal bovine serum

FGF Fibroblast factor

GAPDH Glyceraldehyde-3-phosphate dehydrogenase

GBM Glioblastoma

GDNF Glial cell derived neurotrophic factor

GFP Green fluorescent protein

HB-EGF Heparin-binding EGF-like growth factor

HBMECs Human brain microvascular endothelial cell

H&E Hematoxylin & eosin

HGF Hepatocyte growth factor

HIFα Hypoxia-inducible factor 1-alpha

HUVEC Human umbilical vein endothelial cells

IDH1 Isocitrate dehydrogenase 1

IF Immunofluorescent

IOD Integrated optical density

KLF2/4 Krüppel-like Factor 2

MAPK Mitogen-activated protein kinase

MCP-1 Monocyte chemoattractant protein 1

MEKK MAP kinase kinase kinase

MEME Minimum essential medium Eagle

MGMT Promoter methylation of O6-Methylguanine-DNA methyltransferase

MMP2 Matrix metalloproteinase 2

MMPs Matrix metalloproteinases

MRI Magnetic resonance imaging

MST4 Mammalian STE20-like protein kinase 4

mTOR Mammalian target of rapamycin

MTT 3-(4,5-Dimethylthiazol-2-yl)-2,5-Diphenyltetrazolium Bromide

MVD Microvascular density

NSCLC Non-small cell lung cancer

NVP NVP-BHG712

PBS Phosphate buffered saline

PDCD10 Programmed cell death10

PDGF Platelet-derived growth factor receptor

PDGFR-alpha Platelet-derived growth factor receptor-alpha

p-Erk1/2 Phosphor-extracellular signalregulated kinase 1/2

PI3K Phosphatidyl inositol 3 kinase

PTEN Phosphatase and tensin homolog

RB1 Retinoblastoma protein

RFP Red fluorescent protein

RT^2-PCR Real time Reverse transcription-PCR

RTKs Receptor tyrosine kinases

SDS Sodium dodecyl sulfate

shPDCD10 PDCD10 knockdown

shPDCD10 TCs shPDCD10 GBM cells

shRNA Short hairpin RNA

STK Serine/threonine-protein kinase

STS Stausporine

TBS Tris buffered saline

TCGA The Cancer Genome Atlas

TEMED N,N,N',N'-tetramethyl-ethylen-diamine

TFAR15 TF-1 cell apoptosis related gene 15

TMZ Temozolomide

TP53 Tumor protein p53

VEGF Vascular endothelial growth factor

VEGF-C Vascular endothelial growth factor C

VEGFR Vascular endothelial growth factor receptor

VT Tumor volume

WHO World Health Organization

7.2 Figure titles

Figure 1 Successful transduction of PDCD10 in GBM cells

Figure 2 Knockdown of PDCD10 increased the expression and the kinase activity of EphB4 in GBM cells, which was reversed by the treatment with the specific kinase inhibitor of EphB4 (NVP)

Figure 3 Knockdown of PDCD10 promoted proliferation of T98g cells, which was rescued by the treatment of NVP

Figure 4 Knockdown of PDCD10 enhanced adhesion of T98g cells, which was suppressed by the treatment of NVP

Figure 5 Knockdown of PDCD10 activated migration of T98g cells, which was inhibited by the treatment of NVP

Figure 6 Knockdown of PDCD10 stimulated invasion of T98g cells, which was hindered by the treatment of NVP

Figure 7 Conditioned medium from shPDCD10 T98g cells stimulated HUVECs growth

Figure 8 CM from PDCD10 knockdown GBM cells promoted HUVECs adhesion

Figure 9 CM from shPDCD10-GBM cells enhanced HUVECs migration

Figure 10 CM from shPDCD10-GBM cells stimulated HUVECs migration

Figure 11 Knockdown of PDCD10 promoted tumor progression *in vivo*, which was suppressed by the treatment of EphB4 kinase inhibitor NVP

Figure 12 Knockdown of PDCD10 activated proliferation of U87 cells *in vivo,* which was inhibited by NVP

Figure 13 Knockdown of PDCD10 promoted neo-angiogenesis of U87 cells *in vivo,* which was rescued by NVP

Figure 14 Loss of PDCD10 in GBM cells stimulated the release of proangiogenic factors

7.3 Table titles

Table 1 Primer sequences for RT^2-PCR.

Table 2 Soluble factors detected by protein array.

8. Acknowledgements

First of all, I would like to express all my gratitude to the supervisor

Prof. Dr. rer. nat. Yuan Zhu

for giving me the opportunity to do my MD study under her guidance, supporting me whenever I needed her help and introducing me into the world of science. Throughout my doctoral work, Prof. Zhu taught me how to perform scientific work, present research data in an accurate way, and encouraged me to develop the ability of creativity and new skills. I would also like to thank her for great support in writing thesis and publication and for all the helpful and productive discussions and advices. I would also like to thank Prof. Ulrich Sure for providing me the opportunity to study in his department and for his and Prof. Zhu's supporting to participate in the 69th German Neurosurgery Annual Meetings. In addition, I would like to thank China Office, Medical Faculty, Duisburg-Essen University for providing me the scholarship and supporting my study and life here. I also thank Department of Neurosurgery for the financial support of consumable materials during my work.

I am also deeply indebted to Dr. Anja Prinz, Dr. Kai Zhao and Dr. Christine Haselier for their contributions to establishing knockdown cell lines. Moreover, I would like to thank Dr. Anna-Chrisitin Nickel who patiently answered my questions, made productive discussions and encouraged me when I was lost. I would also like to thank Dr. Tatjana Ryl who helped me to search for useful information and prepare my doctor thesis. I extend sincere thanks to them for German translation in my thesis.

My thanks should also go to Ms. Rita Haase and Mr. Mike Sucker for the kind technical support during my work in the laboratory and I also like to thank them for the nice and friendly atmosphere, making it really comfortable to work with them. Finally, I would like to express my gratitude to my parents and my wife for supporting me throughout my study in Germany.

9. List of publication

1. Xueyan Wan, Changshu Ke , Lili Yin, Ting Lei. Clinical characteristics of pituitary carcinoma: one case report. Chin J of Neurol.2013, 46(4):238-242

2. Xueyan Wan, Yu Xu, Juan Chen, Zhuowei Lei, Shengwen Liu, Chao Gan, Chaoxi Li, Ting Lei. Diagnosis and treatment of pituitary adenoma combined with Rathke's cleft. J of Clinical Nerosurg.2013, 10(3):145-147.

3. Xueyan Wan, Yu Xu, Huaqiu Zhang, Shengwen Liu, Qungen Xiao, Suojun Zhang, Ting Lei. Invasive pituitary adenomas: clinical outcome and treatment strategies. Chin J of Neurosurg.2013, 29(5):451-455.

4. Liu S, Wan X, Wang S, et al. Posttraumatic cerebral infarction in severe traumatic brain injury: characteristics, risk factors and potential mechanisms. Acta Neurochir (Wien). 2015; 157:1697-1704.

5. Wan X, Liu S, Wang S, et al. Elderly Patients with Severe Traumatic Brain Injury Could Benefit from Surgical Treatment. World Neurosurg. 2016; 89:147-152.

6. Wan X, Fan T, Wang S, et al. Progressive hemorrhagic injury in patients with traumatic intracerebral hemorrhage: characteristics, risk factors and impact on management. Acta Neurochir (Wien). 2017;159:227-235.

7. Wan X, Zhao K, Wang S, et al. Is It Reliable to Predict the Outcome of Elderly Patients with Severe Traumatic Brain Injury Using the IMPACT Prognostic Calculator? World Neurosurg. 2017; 103:584-590.

8. Zhang S, Wang S, Wan X, Liu S, Shu K, Lei T. Clinical evaluation of post-operative cerebral infarction in traumatic epidural haematoma. Brain Inj. 2017; 31:215-220.

9. Nickel AC, Wan XY, Saban DV, et al. Loss of programmed cell death 10 activates tumor cells and leads to temozolomide-resistance in glioblastoma. J Neurooncol. 2019; 141: 31-41.

10. Wan XY, Saban DV, Kim SN, et al. PDCD10-deficiency promotes malignant behaviors and tumor growth via triggering EphB4 kinase activity in glioblastoma. Front Oncol. 2020, DOI: 10.3389/fonc.2020.01377.

10. Curriculum Vitae

The curriculum vitae is not included in the online version for data protection reasons.